

Chapter 10

MODELING CAM-FOLLOWER SYSTEMS

10.0 INTRODUCTION

In Chapter 9, a simple kinetostatic model of a cam-follower system was presented. That model is sufficient for determining (and thus avoiding by design) the condition of gross follower jump due to inadequate spring force and/or preload. Properly designed cam-follower systems for industrial machine applications usually do not have follower jump problems, in part because they are operated at controlled speeds. Internal combustion engine valve trains, on the other hand, can experience follower jump (or toss) if the "nut behind the wheel" revs the engine beyond its redline rpm. The "redline" on the tachometer is there to indicate the maximum engine speed allowed before the cam-followers will leave contact with the cams. Modern engines with electronically controlled ignition and fuel injection are usually equipped with a rev limiter that cuts the ignition or fuel supply if the driver tries to exceed the redline rpm.

All cam-follower systems have sufficient elasticity in their components to present the possibility of residual vibrations in operation. These are oscillations of relatively small magnitude within the various links and levers that comprise the follower train. Though these oscillations are small compared to the potential deviation in follower motion that accompanies a gross jump phenomenon from over-revving, they may nevertheless create dynamic problems. In automotive valve trains, vibration of the coils of the return spring, called spring surge, is a common problem. The harmonic content of the cam profile can interact with the natural frequencies of the spring coils at particular engine speeds, causing the coils to vibrate so violently that they impact one another, a condition known as coil clash. In industrial machinery, residual vibrations in the follower train can introduce significant positional error, especially during dwells when the continuing vibration induced by the rise or fall event compromises follower position accuracy. Vibration can also disrupt the phasing of follower motions creating the potential for interference between closely timed and spaced followers driven from different cams.

This chapter presents several dynamic models that are suitable for the determination of dynamic behavior and residual vibrations within cam-follower systems, as well as providing the means to predict follower jump. Some of these models are linear and so their differential equations of motion can be solved analytically. Others include nonlinear or nonconstant terms and so must be solved numerically, typically with a Runge-Kutta, Adams, Bulirsch-Stoer, or other algorithm. In either case, a computer solution is needed. Many commercially available computer programs will solve these equations, e.g., *TKSolver*,* *Mathcad*,† and MATLAB/SIMULINK.‡

10.1 DEGREES OF FREEDOM

A great deal of work has been done in developing dynamic models of cam systems and comparing their simulated data to experimental data over the past fifty years. There is general agreement^{[1],[2],[3],[4]} that a lumped parameter single degree of freedom (SDOF) model is adequate to model most aspects of dynamic behavior of these systems. Koster^[2] developed one-, two-, four-, and five-DOF models of a cam-follower system, using the additional DOF to include the effects of camshaft torsion and bending, backlash, squeeze of lubricant in bearings, camshaft angular velocity variation, and the drive motor characteristic. He concludes that the SDOF model (which correlated well with experiment)

proves to be an adequate tool for predicting the amplitude of the residual vibration of a cam follower driven by a relatively flexible shaft, despite the fact that considerable simplifications have been introduced . . .^[5]

Nevertheless, others have developed multi-DOF lumped-parameter models for this application. Seidlitz^[6] describes a 21-DOF model of a pushrod overhead valve train as shown in Figure 10-1 in which he used one DOF for the camshaft, two for the hydraulic tappet, two for the pushrod, four for the rocker arm, one for the spring retainer, two for the valve, and nine for the valve spring. Two of the dampers were nonlinear. From this extensive numerical simulation that correlated well with experimental measurements he concludes that:

In spite of the presence of some nonlinear damping and three-dimensional motions, a valve train can be viewed as a linear, one-dimensional mechanical system with two resonant frequencies. The first mode is predominately the first axial mode of the valve spring with the highest modal motion at the middle of the valve spring. The second mode is predominately the remainder of the valve train stretching and compressing along its axial length with the highest modal motion at the valve head.^[7]

This recommends a two-DOF model that can separate the spring and follower train.

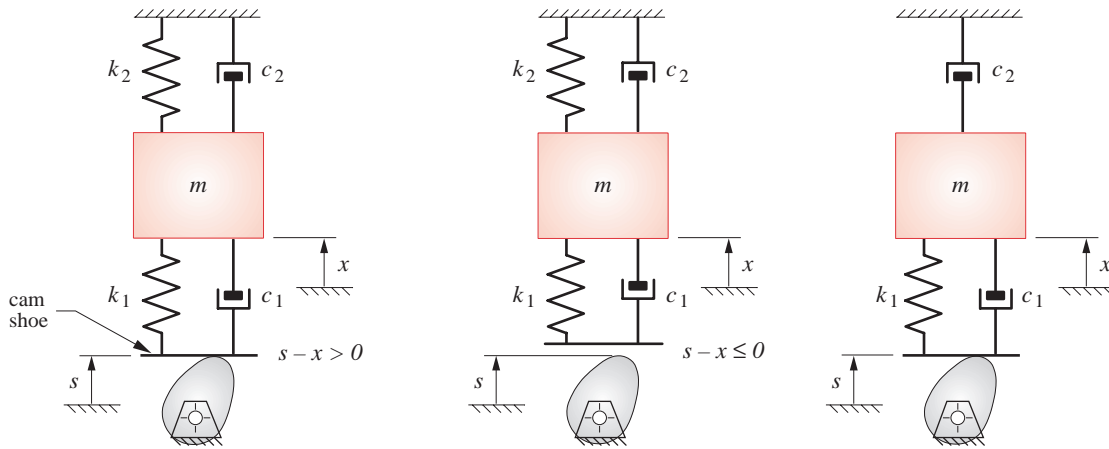
Pisano^[8] used a combined lumped and distributed parameter model of a valve train and confirmed its accuracy experimentally. Regarding the model, he concludes:

The incorporation of a distributed parameter element (helical valve spring) is crucial to the formulation of an accurate predictive model of a high-speed cam-follower system . . . The careful modeling of the valve spring as a distributed parameter (continuum) component is the key to success of the complete dynamic model . . .^[9]

* Universal Technical Services, 1220 Rock St., Rockford, IL 61101. www.uts.com

† Mathsoft Inc., 101 Main St. Cambridge, MA 02142. www.mathsoft.com

‡ The MathWorks Inc., 24 Prime Park Way, Natick, Massachusetts, 01760. www.mathworks.com



(a) Force-closed system (in contact) (b) Force-closed system (jumping) (c) Form-closed system

FIGURE 10-2

Simplest SDOF lumped parameter models of a cam-follower system with return spring (k_2) at end effector

though the presence of backlash allows impact between cam and follower whenever the sign of the cam-follower force changes sign. This is termed crossover shock.

In both cases the input to the system is the designed cam displacement $s(t)$ and the output is the motion $x(t)$ of the mass. Note that as long as the force between cam and shoe is > 0 in the force-closed system the cam and follower remain in contact. If not, the follower will jump off the cam.

Force-Closed Models

Figure 10-3 shows the model of Figure 10-2a and its free body diagram. The equation of motion for the system is found from Newton's second law:

$$\begin{aligned} \sum F &= m\ddot{x} \\ k_1(s-x) + c_1(\dot{s} - \dot{x}) - k_2x - c_2\dot{x} &= m\ddot{x} \\ \ddot{x} + \frac{c_1 + c_2}{m}\dot{x} + \frac{k_1 + k_2}{m}x &= \frac{k_1}{m}s + \frac{c_1}{m}\dot{s} \end{aligned} \quad (10.1a)$$

where s = cam profile input displacement and x = cam follower output displacement.

With the following substitutions, equation 10.1a can be put in a form that involves natural frequencies and damping ratios.

$$\begin{aligned} \frac{c_1 + c_2}{m} &= 2\zeta_2\omega_2 & \frac{k_1 + k_2}{m} &= \omega_2^2 & \frac{k_1}{m} &= \omega_1^2 & \frac{c_1}{m} &= 2\zeta_1\omega_1 \\ \ddot{x} + 2\zeta_2\omega_2\dot{x} + \omega_2^2x &= \omega_1^2s + 2\zeta_1\omega_1\dot{s} \end{aligned} \quad (10.1b)$$

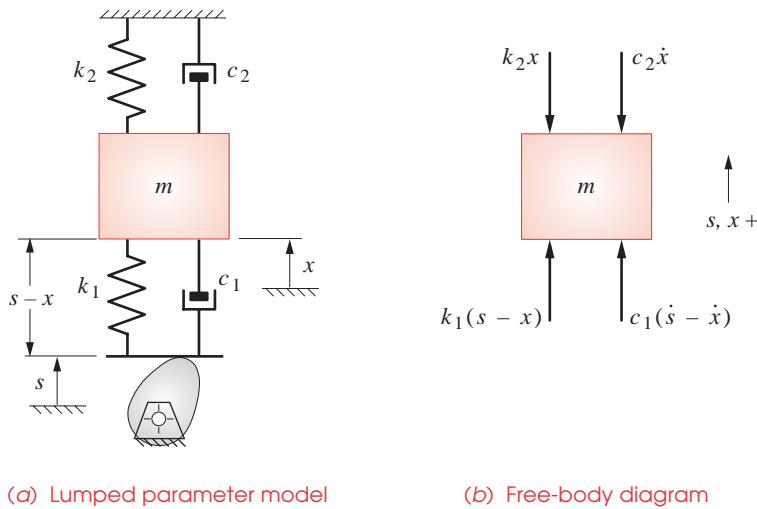


FIGURE 10-3

SDOF lumped parameter model and free-body diagram of a force-closed cam-follower system with return spring k_2 at end effector

Note that in this model, the springs k_1 and k_2 combine in parallel to compute ω_2 , because each has an independent path to ground, k_2 directly and k_1 through the cam (as long as no follower jump occurs). Program DYNACAM solves the model in Figure 10-3a.

After jump occurs, the system m, k_2, c_2 is in free vibration according to:

$$\ddot{x} + \frac{c_2}{m} \dot{x} + \frac{k_2}{m} x = 0 \quad (10.1c)$$

the solution to which was derived in Chapter 9 (see equation 9.5).

Wiederrich^[10] points out that the vibration of the system can be more clearly defined by creating a relative vibration parameter r that defines the deviation of the instantaneous position x versus its static deflection x_s from

$$r = x_s - x \quad (10.2a)$$

The static deflection can be found by setting the time derivatives in equation 10.1b to zero

$$x_s = \frac{\omega_1^2}{\omega_2^2} s \quad (10.2b)$$

Combine 10.2a and 10.2b to get an expression for relative vibration in terms of s and x

$$r = \frac{\omega_1^2}{\omega_2^2} s - x \quad (10.2c)$$

Substitute equation 10.2c and its derivatives in 10.1b to obtain the equation of motion in terms of the relative vibration r .

$$\ddot{r} + 2\zeta_2\omega_2\dot{r} + \omega_2^2 r = \frac{\omega_1^2}{\omega_2^2} \ddot{s} + 2(\omega_1\zeta_2 - \omega_2\zeta_1) \frac{\omega_1}{\omega_2} \dot{s} \quad (10.2d)$$

Equation 10-2d shows that for systems with low damping (as these are) **the factor that has the most influence on vibration is the cam acceleration**. This further reinforces the points made in the early chapters that the higher derivatives of follower motion are the most important in respect to system dynamics.

Form-Closed Model

The equation of motion for the model shown in Figure 10-2c is:

$$\ddot{x} + \frac{c_1 + c_2}{m} \dot{x} + \frac{k_1}{m} x = \frac{k_1}{m} s + \frac{c_1}{m} \dot{s} \quad (10.3a)$$

With the following substitutions, it can be put in a different form that involves natural frequencies and damping ratios.

$$\frac{k_1}{m} = \omega_n^2 \quad \frac{c_1 + c_2}{m} = 2\zeta_2\omega_n \quad \frac{c_1}{m} = 2\zeta_1\omega_n$$

$$\ddot{x} + 2\zeta_2\omega_n\dot{x} + \omega_n^2 x = \omega_n^2 s + 2\zeta_1\omega_n\dot{s} \quad (10.3b)$$

The damping ratio ζ_2 in a form-closed (track) cam is typically so low (being mainly internal material damping) that it can be considered to be zero. Then:

$$\ddot{x} + \omega_n^2 x = \omega_n^2 s + 2\zeta_1\omega_n\dot{s} \quad (10.3c)$$

BACKLASH In a form closed cam, the backlash will be taken up whenever the force between cam and follower reverses direction. This is called crossover shock and can create potentially severe impact forces. With negligible damping, an impact force F_i can be roughly estimated by conservation of energy as^[11]

$$F_i \cong v_i \sqrt{mk} \quad (10.4a)$$

where v_i is the impact velocity, m is the striking mass, and k is the spring constant of the struck system.

Koster^[2] reports on a method (attributed to Van der Hoek) to estimate the impact velocity in a track cam from:

$$v_i \cong \frac{1}{2} (j_{t_i})^{1/3} (6y_i)^{2/3} \quad (10.4b)$$

where j_{t_i} is the value of the jerk of the follower motion at the time of impact t_i , and y_i is the amount of backlash present in the cam track at that position. The times of impact (force reversals) can be determined from the simulation using equation 10.3. They typically will be close to points of acceleration reversal. The amount of backlash can be estimated at the design stage from nominal fits in joints and expected tolerances of manu-

facture of cam and roller follower. For an existing system, backlash is easily measured with a dial indicator. It can be seen from equations 10.4 that for any amount of irreducible backlash, the impact force can be reduced by choosing a cam function with lower values of jerk at the points of acceleration reversal. Also, wear will increase backlash over time.

10.3 TWO-MASS, ONE- OR TWO-DOF, NONLINEAR DYNAMIC MODEL OF A VALVE TRAIN

The simple models described in the previous section are considered to be adequate for many cam-follower systems such as valve trains where the spring is at the end effector, particularly if the mass at the end effector is relatively large compared to the mass of the follower train components closer to the cam, if jump is unlikely, damping is not dominated by coulomb friction, and if the follower is never deliberately held off the cam (such as during a dwell). If these conditions are not true, then a more elaborate model is needed to give a better prediction of follower dynamics.

Barkan^[1] developed a model for the automotive valve train that, with slight refinements by others,^{[3],[4]} has proven to quite accurately predict the behavior of this more dynamically complicated cam-follower system.

Barkan showed that including a coulomb damper as well as a viscous damper significantly improved the model. The viscous damping ratio was assumed to be between 0.02 and 0.15, based on the literature. A coulomb friction coefficient of 0.2 was used. Barkan also includes the gas force acting on the valve head.

Akiba added a second lumped mass at the cam.^[3] This better predicts cam contact force, and thus jump, than the single mass model.^[4] The two-mass model also becomes a 2-DOF system after jump occurs, giving a more realistic and accurate simulation. The model also provides for contact between valve and valve seat at closure.

For proper engine operation, a valve train must ensure tight closure of the valve during dwell, both to eliminate blowby and to give the valves (especially the exhaust valve) good coupling for heat transfer to the valve seat. This is accomplished by either maintaining a deliberate clearance (valve lash) between the cam follower and cam during the dwell, or providing a hydraulic lash adjuster as a compliant link between the two. This also compensates for the thermal expansion of the follower train at operating temperature.

An analogous condition is often encountered in industrial machinery when a follower train is brought back to a "hard stop" on the ground plane just short of the low dwell. A hard stop is sometimes needed when the cam is interrupted and leaves the follower for part of the low dwell or it may be needed to guarantee follower train position during the low dwell to a greater mechanical accuracy than can be obtained from the cam, given the stack-up of assembly tolerances and dynamic deflections.

In both of these situations, there is an impact event when the follower train hits the hard stop (or valve seat) with some velocity, and again at the beginning of the rise as the cam encounters the stationary follower with some velocity. The cam design in these cases often contains constant velocity "ramps" at the beginning and end of the rise to control the magnitude of the impact velocities over a range of tolerance of the impact point.

The 1- or 2-DOF, two-mass model^[4] is shown in Figure 10-4a. Its equation of motion for the condition of continuous contact between mass m_1 and the cam is:

$$m_2\ddot{x} + c\dot{x} + (k_1 + k_2)x - k_1 \frac{\dot{y}}{|y|} \mu |x| = m_2\ddot{z} + k_2(z + z_i) \quad (10.5a)$$

where $x = z - y$ and z_i is the initial deflection of return spring k_2 at assembly (preload deflection).

When mass m_1 and the cam separate, equation 10.5a still applies, but z is unknown. A second equation is then needed, involving the force between cam and follower:

$$F_c = m_1\ddot{z} + c\dot{x} + k_1x \quad (10.5b)$$

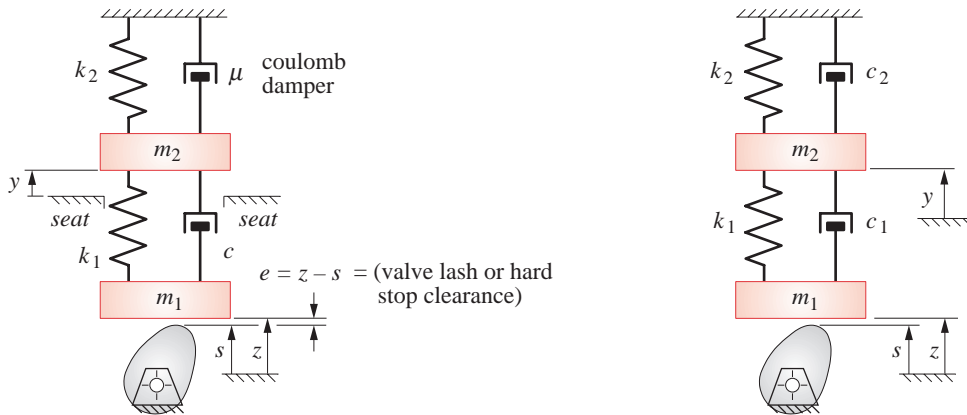
F_c will be zero when mass m_1 is not in contact with the cam.

The simplified two-mass model of Figure 10-4b eliminates the nonlinear coulomb damper and the valve seat impact. Its equations for the condition of contact between cam and follower mass m_1 ($z = s$) are:

$$\ddot{x} = \ddot{z} + \frac{k_2}{m_2}(z - z_i) + \frac{c_2}{m_2}\dot{z} - \frac{c_1 + c_2}{m_2}\dot{x} - \frac{k_1 + k_2}{m_2}x \quad (10.5c)$$

$$F_c = m_1\ddot{z} + c_1\dot{x} + k_1x \quad (10.5d)$$

To solve either of the systems in Figure 10-4, equation 10.5a or 10.5c is first solved for displacement x , then equation 10.5b or 10.5d is solved for F_c . If F_c is positive, then the value of x is valid (Case 1). If F_c is negative, then separation has occurred and equations 10.5a and b (or 10.5c and d) are solved simultaneously with F_c set to zero at that time step (Case 2), maintaining the initial velocity and displacement conditions. As the



(a) Dresner & Barkan's two-mass valve-train model

(b) Simplified two-mass model

FIGURE 10-4

One- or two-DOF two-mass model of a cam-follower system with return spring (k_2) at end effector (4)

solution continues for additional time steps, s and z are compared at each step. When z becomes $\leq s$, the cam and follower have regained contact and the solution reverts to Case 1, maintaining the initial condition for dx/dt but changing the initial condition for dz/dt to match the cam velocity. This assumes a coefficient of restitution of zero on impact, which does not accurately model the impact event but is valid after the follower stops bouncing on the cam. When a transition is made from one case to the other, the time at which F_c changes sign must be found by iteration in order to maximize accuracy.^[4]

Figure 10-5 shows displacement and acceleration data from a valve train modeled as in Figure 10-4a. The simulated, theoretical, and experimentally measured curves are shown to be quite similar.^[1] Program DYNACAM solves the model in Figure 10-4b, but does not attempt to track the follower motion after separation because that is an unacceptable condition requiring redesign of the joint closure system.

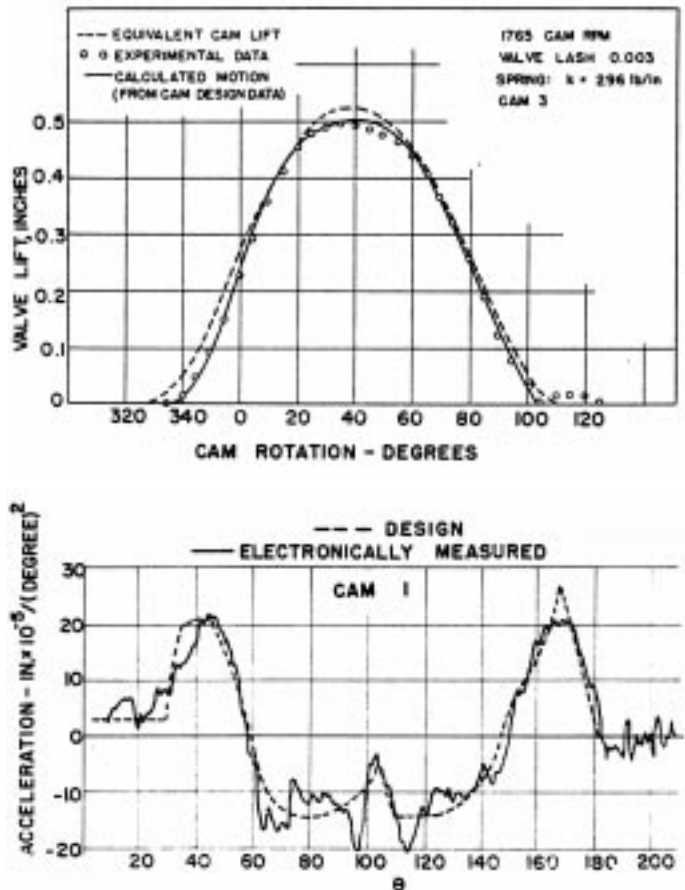


FIGURE 10-5

Simulated, theoretical, and experimental valve train displacement and acceleration ⁽¹⁾

10.4 MULTI-DOF DYNAMIC MODEL OF A VALVE TRAIN

Seidlitz^[6] built the 21-DOF model of a valve train shown in Figure 10-1 (p. 265). A brief description of his modeling techniques and assumptions will be given here as a guide to the reader wishing to create a multi-DOF model of a different cam-follower system. More detail can be found in the original reference, which is quite complete.

Springs and/or dampers attach the model to ground at the camshaft, hydraulic tappet, rocker arm center, valve center, valve head, and the bottom of the valve spring. The camshaft was modeled as one mass, spring, and damper system, with its mass being that of one cam lobe plus half of the remaining mass between the cam bearings. Its spring rate was that of the camshaft in bending at the cam lobe.

The hydraulic tappet model had two masses, one spring, and two dampers. The spring rate of the tappet's oil column was "backed out" of the model (when run) by adjusting its value to get good correlation with experimental data. This method is commonly used in dynamic modeling to estimate values of elements (particularly dampers) that are difficult to either calculate or measure directly. A dead band was also built into the model calculation to simulate the lost motion associated with the tappets's internal check valve.

The pushrod was modeled as two masses, each half its total mass, three springs, and three dampers. The end springs each had the same stiffness but were twice the stiffness of the center spring. The combined spring rate of the three springs in series equaled that of the actual pushrod.

The rocker arm was modeled as three masses, one inertia, three springs, and four dampers. One mass was placed at each end of the arm and one at its center. The rotational inertia value applied at the center mass was the actual arm's inertia minus the effective inertia of the two end masses. Each end spring represented the effective spring rate from the center of the arm to that end. These values were determined by a static force-deflection measurement on the rocker arm. (Nowadays, if a solids model of a proposed design exists, it is a short step to make FEA models of its elements such as rocker arms and determine their spring rates before any metal is cut.)

The valve spring was modeled as nine masses, ten springs, and ten dampers. The total spring mass was divided by the number of coils, and one coil's worth assigned to each of the end masses. The remaining mass was divided equally among the remaining seven lumped masses. The two end springs were made ten times stiffer than the middle springs. This made the middle springs 8.2 times as stiff as that of the actual valve spring. Each value could be entered separately in the model allowing any combination of masses, springs, and dampers to mimic alternate spring designs. Coil-to-coil contact was simulated and when coils touched in the simulation, their spring and damper values were increased by a hundredfold. By varying clearances between coils in the model, a variable rate spring could be simulated. (A variable-rate valve spring typically is wound with a varying coil pitch. As the spring compresses, the close-spaced coils contact one another and thus increase the spring rate dynamically.)

Camshaft speed was assumed constant. The cam lift profile was entered into the model as an array of lift values at half-degree intervals and smoothed with a 5th-order

polynomial for sampling at the model's calculation times. The system equation was written in matrix form:

$$[\mathbf{M}]\ddot{x} + [\mathbf{C}]\dot{x} + [\mathbf{K}]x = F(t) \quad (10.6)$$

where \mathbf{M} is the mass matrix, \mathbf{C} is the damping matrix, and \mathbf{K} is the stiffness matrix for the system. This matrix equation was solved with a custom-written computer program. Damping coefficients that are difficult to determine independently were adjusted to obtain good correlation of the simulation with experimental measurements made of the actual valve train. Once a model such as this is "tuned" to match experimental data, it becomes a tool that can be used to investigate the dynamic effects of proposed design changes, or entirely new but similar designs, in advance of their implementation in hardware.

Figure 10-6 shows a sample of the simulated and experimental data, superposed. Good correlation between the simulation and experiment can be seen in the acceleration plots of valve head and pushrod. The pushrod force shows reasonable correlation, as does the acceleration at the middle of the spring. While a great deal of effort is required to create and verify a model of this complexity, when done, it can give a wealth of dynamic information about that system and about similar systems yet to be built.

10.5 ONE-MASS MODEL OF AN INDUSTRIAL CAM-FOLLOWER SYSTEM

The models described in the previous sections are all directed at the automotive valve train application, particularly the overhead-valve pushrod type. They have been shown to agree quite closely with experimental data from those mechanisms. However, these models may not provide a good representation of the typical industrial cam-follower train as used in automated machinery. These systems often look like Figure 10-7 where the follower spring (or air-cylinder "spring") connects the follower to ground close to the cam rather than at the end effector, as it is in the case of the overhead valve train of Figure 10-1.* Figure 10-8 shows SDOF models and free-body diagrams of this system for the form-closed and force-closed cam cases, their difference being the additional spring needed to maintain contact of the cam joint in the latter case, along with its associated damping.

THE FORM-CLOSED CASE Figure 10-8a shows an example of the classic, base-excited SDOF system found in any introductory text on vibration theory if we assume that the damping between the mass and ground is negligible. Its system equation is found from summing forces on the free-body diagram (FBD) of Figure 10-8a.

$$\ddot{x} + \frac{c}{m}\dot{x} + \frac{k}{m}x = \frac{k}{m}s + \frac{c}{m}\dot{s} \quad (10.7a)$$

where :

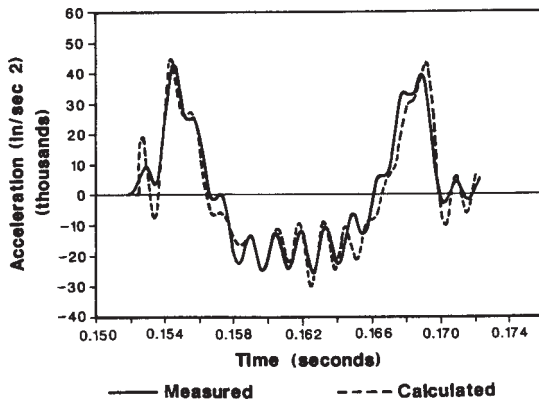
$$\frac{k}{m} = \omega_n^2, \quad \frac{c}{m} = 2\zeta\omega_n$$

then :

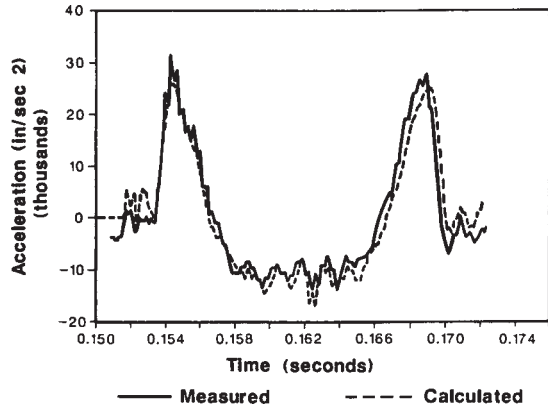
$$\ddot{x} + 2\zeta\omega_n\dot{x} + \omega_n^2x = \omega_n^2s + 2\zeta\omega_n\dot{s} \quad (10.7b)$$

Its response to an harmonic excitation of the base, $s(t) = h \sin(\omega t)$, is given by:

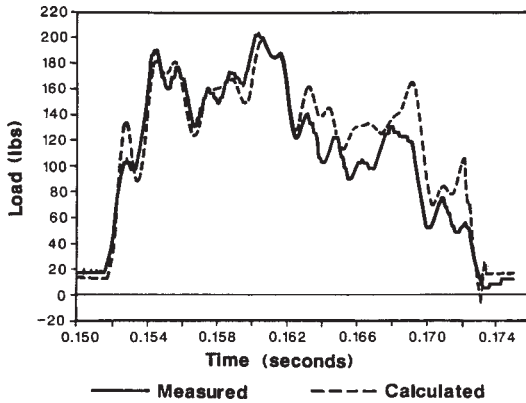
* Note that some industrial cam-follower trains have the joint closure spring placed at the end effector in order to load all the joint clearances in one direction and take out the backlash in the system. If this is done, then the valve train model gives a better representation of its dynamic behavior. Program DYNACAM provides both dynamic models for analysis.



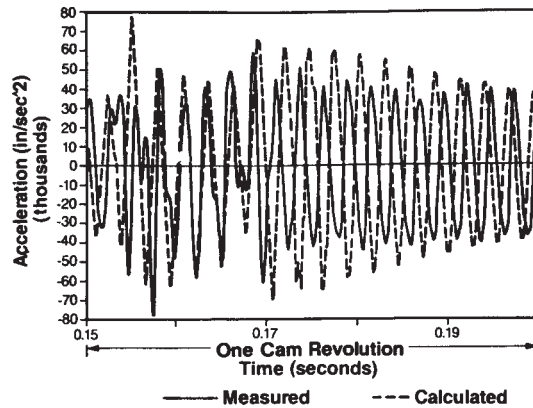
(a) Acceleration of valve head



(b) Acceleration at bottom of pushrod



(c) Force in pushrod



(d) Acceleration at middle of valve spring

FIGURE 10-6

Simulated and experimental dynamics of an overhead valve train at 2400 engine rpm ⁽⁶⁾

$$x = A h \sin(\omega t - \phi)$$

where :

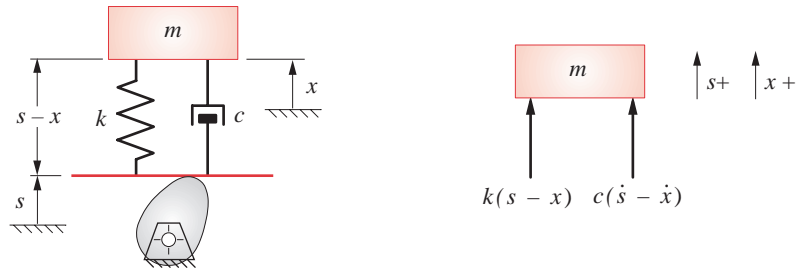
$$A = \text{amplitude ratio} = \frac{x}{h} = \frac{1 + (2F_r \zeta)^2}{\sqrt{(1 - r^2)^2 + (2F_r \zeta)^2}}$$

(10.7c)

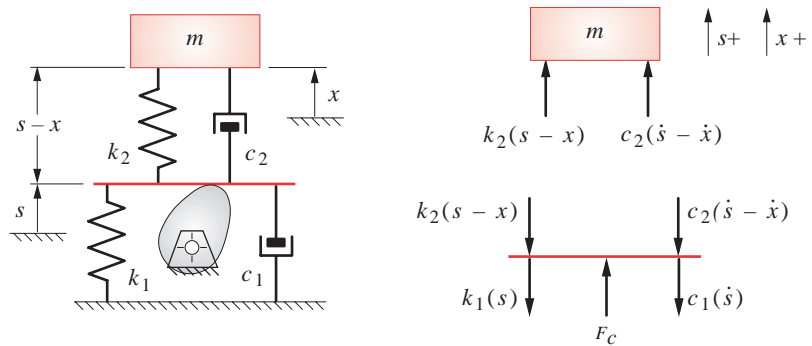
$$\phi = \text{phase angle} = \arctan \left[\frac{2\zeta F_r^3}{1 + (4\zeta^2 - 1)F_r^2} \right]$$

where :

$$F_r = \text{frequency ratio} = \frac{\omega}{\omega_n}$$



(a) Form-closed system and free-body diagram



(b) Force-closed system and free-body diagrams

FIGURE 10-8

SDOF models and free-body diagrams (FBD) of a typical industrial cam-follower system

These functions are plotted in Figure 10-9 over a range of frequency ratios F_r with several different damping ratios ζ .

Note in Figure 10-9 that at the typical damping ratio for these systems of $\zeta = 0.05$, the amplitude ratio, or system gain at resonance is about 10. Note also that with essentially zero damping, the phase relationship between the forcing function s and the response x abruptly shifts from in-phase ($\phi = 0^\circ$) to opposite phase ($\phi = 180^\circ$) at resonance. With low damping ratios, there is a more gradual phase change as the system approaches and passes through resonance, shifting 160° at $\zeta = 0.05$ and 100° at $\zeta = 0.25$.

THE FORCE-CLOSED CASE Figure 10-8b shows a force-closed system that requires an additional spring k_1 to keep the joint from separating. We assume that the damping between the mass and ground is negligible. This system has two possible operational modes. As long as contact is maintained at the cam joint, it behaves essentially similar to the form-closed system of Figure 10-8a. In that condition, the joint-closure spring k_1 does not contribute to its vibratory behavior and the system's natural frequency is only a function of m and k_2 . If the joint separates, then the system natural frequency abruptly switches to a lower value since k_1 is usually significantly smaller than k_2 . Because the two springs are then in series, the lower k value dominates and k_1 is typically much less than k_2 .

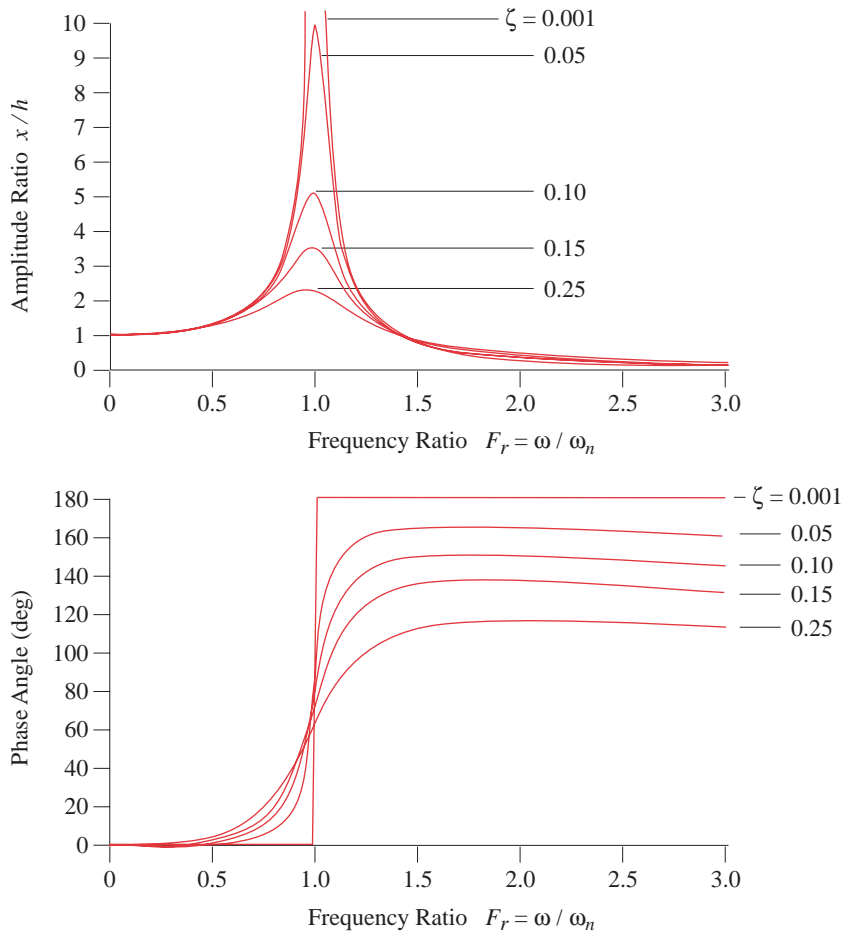


FIGURE 10-9

Amplitude ratio and phase angle of a harmonically base-excited SDOF system

If we assume that contact between cam and follower is somehow maintained at all times, then the system equation is the same as that of equation 10.7, repeated here using notation consistent with Figure 10-8b.

$$\ddot{x} + \frac{c_2}{m} \dot{x} + \frac{k_2}{m} x = \frac{k_2}{m} s + \frac{c_2}{m} \dot{s} \tag{10.8a}$$

where :

$$\frac{k_2}{m} = \omega_2^2, \quad \frac{c_2}{m} = 2\zeta_2 \omega_2$$

then :

$$\ddot{x} + 2\zeta_2 \omega_2 \dot{x} + \omega_2^2 x = \omega_2^2 s + 2\zeta_2 \omega_2 \dot{s} \tag{10.8b}$$

If the joint separates, then the system equation becomes:

$$\ddot{x} + \frac{c_{eff}}{m} \dot{x} + \frac{k_{eff}}{m} x = \frac{k_{eff}}{m} s + \frac{c_{eff}}{m} \dot{s} \tag{10.9a}$$

* This analysis assumes that the internal damping values (c 's) of the elements are very small and vary approximately proportionally to the stiffnesses (k 's) of the respective elements to which they apply. Because damping is typically small in these systems, its effect on the equivalent spring rate is small, but the reverse is not true since high stiffness will affect damping levels. A very stiff element will deflect less under a given load than a less stiff one. If damping is proportional to velocity across the element, then a small deflection will have small velocity. Even if the damping coefficient of that element is large, it will have little effect on the system due to the element's relatively high stiffness. A more accurate way to estimate damping must take the interaction between the k 's and c 's into account. For n springs k_1, k_2, \dots, k_n in series, placed in parallel with n dampers c_1, c_2, \dots, c_n in series, the effective damping can be shown to be:

$$c_{eff} = k_{eff} \sum_{i=1}^n \frac{c_i}{k_i^2}$$

As a practical matter, however, it is usually quite difficult to determine the values of the individual damping elements that are needed to do a calculation such as shown above and in equation (h) on p. 196. Section 9.3 (p. 227) presents a relatively simple method to experimentally determine an approximate overall damping value for an entire system.

$$\text{where: } * \quad k_{eff} = \frac{k_1 k_2}{k_1 + k_2} \quad c_{eff} = \frac{c_1 c_2}{c_1 + c_2} \quad \frac{k_{eff}}{m} = \omega_1^2 \quad \frac{c_{eff}}{m} = 2\zeta_1 \omega_1$$

$$\text{then:} \quad \ddot{x} + 2\zeta_1 \omega_1 \dot{x} + \omega_1^2 x = \omega_1^2 s + 2\zeta_1 \omega_1 \dot{s} \quad (10.9b)$$

Program DYNACAM solves both of the models in Figure 10-8 (p. 276).

This system, though of only one DOF, has two natural frequencies, one when in contact, and another when separated. The question then becomes: under what conditions will it separate? Looking at Figure 10-9 (p. 277), which depicts the in-contact case, it would appear that, with the damping typical in these systems ($\zeta = 0.05$ to 0.10), one could operate at frequency ratios lower than about $\omega_2 / 3$ and expect no separation, provided that the closure spring rate k_1 and preload had been properly selected by the kinetostatic technique shown in Chapter 9 in order to avoid gross kinematic jump.

But what will happen if the operating speed ω chosen on that basis happens to be close to, or above, the lower, separation natural frequency ω_1 of the system? This is entirely possible if the follower train is stiff compared to the closure spring ($k_2 \gg k_1$). This situation is both common and desirable in cam-follower systems. We want the stiffest possible follower train in order to minimize the dynamic error ($s - x$). If k_2 were infinite, then x would equal s , giving zero error. We also do not want the closure spring stiffness k_1 to be any greater than is needed to prevent kinematic jump, because its force, in part, determines the stresses in the cam and follower.

Figure 10-10 shows the two natural frequencies of a system like that in Figure 10-8b (p. 276). The in-contact natural frequency ω_2 is shown higher than the separation natural frequency ω_1 as described above. If the operating frequency ω is made about $1/3$ of ω_2 , then, as depicted in the figure, the system has to pass through ω_1 on start-up; but, ω_1 does not exist as long as contact is maintained. However, if the follower separates from the cam even for an instant as it passes through ω_1 , the phase of the output response x will shift from 0 to 100° or greater (depending on ζ_1) with respect to the input excitation s as shown in Figure 10-9b, and it will begin to resonate at ω_1 . This will cause follower bounce. Therefore, the design constraint for this system is that it should not be allowed to operate too close to the separation natural frequency ω_1 . The smaller the frequency

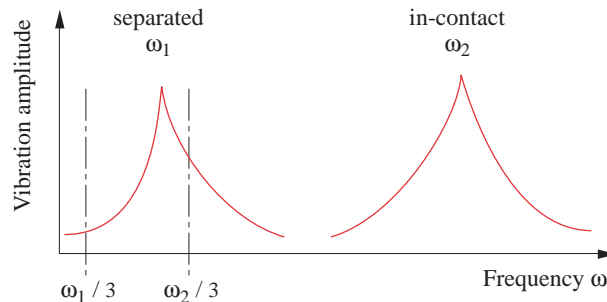


FIGURE 10-10

Separated and in-contact natural frequencies of the system of Figure 10-8b

ratio ω / ω_1 the better. Usually a ratio of about $\omega_1 / 3$ or less will be sufficient to avoid separation and follower jump. The follower spring stiffness k_1 , rather than the follower train stiffness k_2 , then limits the system operating speed ω .

10.6 TWO-MASS MODEL OF AN INDUSTRIAL CAM-FOLLOWER SYSTEM

A better model for the type of system shown in Figure 10-7 is the two-mass model shown in Figure 10-11. This model takes into account that the mass of the system is roughly divided between the cam-follower arm and the end effector, which are connected by relatively lighter connecting rods. The model has two masses, m_1 and m_2 , one at the cam and one at the end effector. Note that m_1 is directly connected to ground by the follower spring k_1 and damper c_1 , while mass m_2 is "piggybacked" on mass m_1 through the stiffness of the follower train k_2 and damper c_2 .

It requires some engineering judgment to appropriately lump the distributed mass of all the links in the system into m_1 and m_2 . Let common sense prevail. For example, in Figure 10-7 (p. 275), lump the mass of the follower arm, roller follower, and half the mass of the connecting rod into m_1 at the cam, properly taking into account all lever ratios as described in Chapter 8. Then lump the mass of the bellcrank, all end effector mass (tooling), and half the connecting rod into m_2 . The spring in the system is easily divided. The actual return spring is k_1 and the combined effective stiffness of the follower train components is k_2 . The damping is typically estimated by selecting appropriate damping ratios based on experience or on measurement as described in Chapter 9.

As with the previous one-mass model, if contact between cam and follower is maintained, this displacement-driven system has one DOF, expressed as x . However, if the cam and follower separate, the system then has two DOF. Moreover, the two DOFs are coupled. Note that when cam and follower separate, this system is similar to the classic vibration absorber wherein a mass-spring combination is added to a (presumed) SDOF

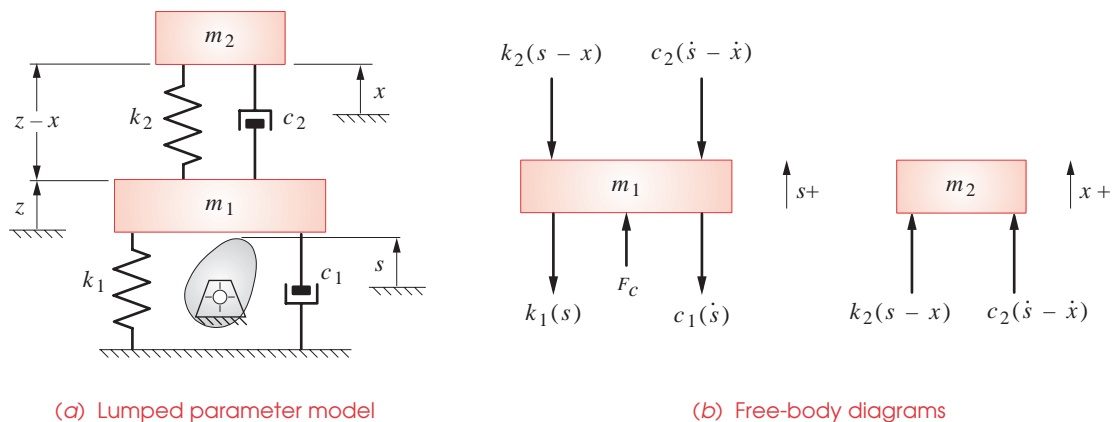


FIGURE 10-11

Two-DOF lumped parameter model and free-body diagrams of the cam-follower system in Figure 10-7

system (see Figure 9-1 on p. 214) in order to split its original single natural frequency into two frequencies Ω_1 and Ω_2 , one above and one below the original natural frequency as shown in Figure 10-12a. In that application, the parameters m_2 and k_2 are carefully selected to "tune" the system such that the vibratory response at the original SDOF natural frequency ω_0 becomes essentially zero, its energy having been "absorbed" into the two new frequencies Ω_1 and Ω_2 as shown in Figure 10-12b.

In our case, the parameters m_1, m_2, k_1, k_2 are essentially "what they are" within the range of our design freedom, and so we will not have a system "tuned" to any particular frequency. However, ω_1 , the lower of the two natural frequencies of this two-DOF system, will always be smaller than the ω_0 of an SDOF model of the same system that assumed the follower train to be rigid (i.e., $k_2 = \infty$), and ω_2 will always be larger than ω_0 .

$$\omega_0 = \sqrt{\frac{k_1}{m_1 + m_2}} \quad (10.10)$$

Thus, a similar situation exists with this two-mass model as with the one-mass model of the previous section. That is, when firmly in contact at the cam joint, it has one, relatively high natural frequency (due to the follower train stiffness k_2), but if perturbed to separate, it immediately shifts to a two-DOF mode in which both new frequencies are different, and one is lower, than the in-contact natural frequency,

Each stage of the model, if independent of the other, would have its own undamped natural frequency as defined by:

$$\omega_1 = \sqrt{\frac{k_1}{m_1}} \quad \omega_2 = \sqrt{\frac{k_2}{m_2}} \quad (10.11a)$$

The two undamped natural frequencies of the coupled system after separation are then:

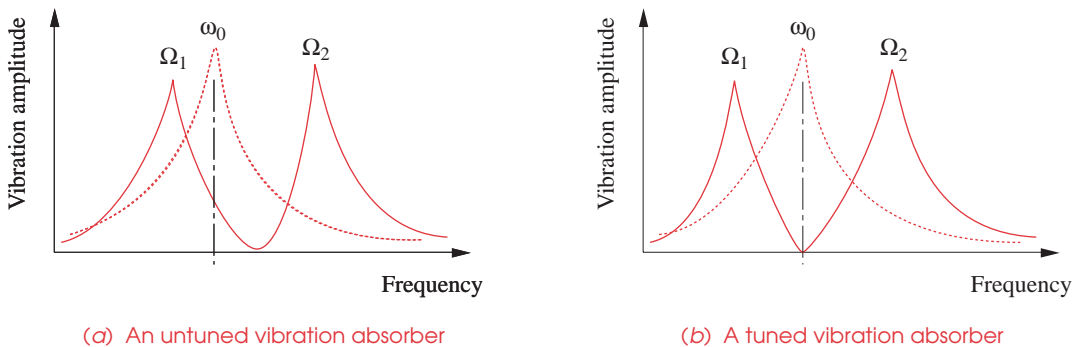


FIGURE 10-12

Frequency response of an SDOF system, with and without a vibration absorber, untuned (a) and tuned (b)

$$\Omega_{1,2} = \frac{\omega_1}{\sqrt{2}} \sqrt{1 + q^2(1+u) \pm \sqrt{q^4(1+u)^2 + 2(u-1)q^2 + 1}} \quad (10.11b)$$

where :

$$q = \frac{\omega_2}{\omega_1} \quad u = \frac{m_2}{m_1}$$

Note that both Ω_1 and Ω_2 are functions of the mass ratio m_2/m_1 and the frequency ratio ω_2/ω_1 , which includes the spring rates k_1 and k_2 .*

Summing forces and applying Newton's 2nd law to the free-body diagrams of Figure 10-11 gives, for the in-contact case:

$$\begin{aligned} m_2 \ddot{x} &= c_2(\dot{z} - \dot{x}) + k_2(z - x) \\ \ddot{x} &= \frac{c_2}{m_2} \dot{z} + \frac{k_2}{m_2} z - \frac{c_2}{m_2} \dot{x} - \frac{k_2}{m_2} x \\ \ddot{x} &= 2\zeta_2 \omega_2 \dot{z} + \omega_2^2 z - 2\zeta_2 \omega_2 \dot{x} - \omega_2^2 x \end{aligned} \quad (10.12a)$$

where, if contact is maintained, $z = s$. The contact force F_c is found from:

$$\begin{aligned} m_1 \ddot{z} &= F_c - c_1 \dot{z} - k_1 z - c_2(\dot{z} - \dot{x}) - k_2(z - x) \\ F_c &= m_1 \ddot{z} + (c_2 + c_1) \dot{z} + (k_2 + k_1) z - c_2 \dot{x} - k_2 x \end{aligned} \quad (10.12b)$$

When separation occurs, the contact force F_c becomes zero.

To solve this system, first assume that cam and follower are in contact, ($z = s$), and solve equation 10.12a for x . Use the value for x at that time step to find F_c from equation 10.12b. If $F_c > 0$, then the cam and follower are in contact at that time and the computed value of x is valid. If $F_c < 0$, then separation has occurred, $z > s$ and the computed value of x is invalid. Then set F_c to zero and solve equations 10.12a and b simultaneously for x and z . Continue this second solution approach, testing z against s at each time step. When $z \leq s$, contact has reoccurred, and equation 10.12a can again be used alone to solve for x until a negative value of F_c is again encountered. Thus the solution must switch between the two solution cases based on the sign of F_c . Note also that when the solution is switched from one stage to the other, the most recent values of x , z and their derivatives must be used as initial conditions for the next stage of the solution.

From a practical standpoint, since separation of cam and follower is generally unacceptable in these systems, the solution process could be aborted when the force goes negative and the designer then prompted to modify the system parameters to correct the problem. For example, increasing the stiffness and/or reducing the mass of the follower system may cure the problem as will increasing the stiffness or preload of the closure spring. Redesigning the cam function to reduce the negative peak acceleration will also improve the situation. Program DYNACAM solves the two-mass model of Figure 10-11 as described in this paragraph.

* As an aside, the deliberate addition of tuned vibration absorbers to a cam-follower system such as is shown in Figure 10-7 can be a very effective way to reduce vibration at any operating speeds that are close to the system's natural frequencies. In fact, one could introduce two such mass-spring absorbers to the system of Figure 10-7, as modeled in Figure 10-11, one mounted on mass m_1 and another mounted on mass m_2 to tune their respective responses to zero at the operating speed.

10.7 SOLVING SYSTEM DIFFERENTIAL EQUATIONS

The closed-form solution to the classic linear, second-order, constant-coefficient ordinary differential equation (ODE) was presented in Chapter 9. That solution is only valid for that particular type of ODE. Though equations 10.1 are in that category, other models of cam follower systems involve nonconstant and nonlinear coefficients and so cannot be solved by traditional closed-form analytical methods. For such equations, which occur frequently in the modeling of dynamic systems, a numerical method of solution is needed. Many such algorithms exist. The Runge-Kutta methods are perhaps the best known, but there also are other methods that may be superior in some instances.^[21]

Block Diagram Solution—Simulink/MatLab

Many computer packages are now available that will solve even complicated differential equations numerically (and symbolically in some cases). One such is MATLAB which contains a simulation package called SIMULINK. This "front-end" to the MATLAB computational engine provides a set of graphical icons for the assembly of a block-diagram solution to any ODE, including ones with nonlinear or nonconstant coefficients. Execution of the model from SIMULINK causes the compilation of the necessary MATLAB commands to solve the system using one of several selectable numerical integration algorithms. In this case, the Adams algorithm appeared to give the best results.

A block diagram is a graphical depiction of the differential equation. To solve an ODE with a numerical algorithm, it is necessary to rearrange the equation so as to be explicit in the highest derivative. Equations 10.1a and b then become, respectively:

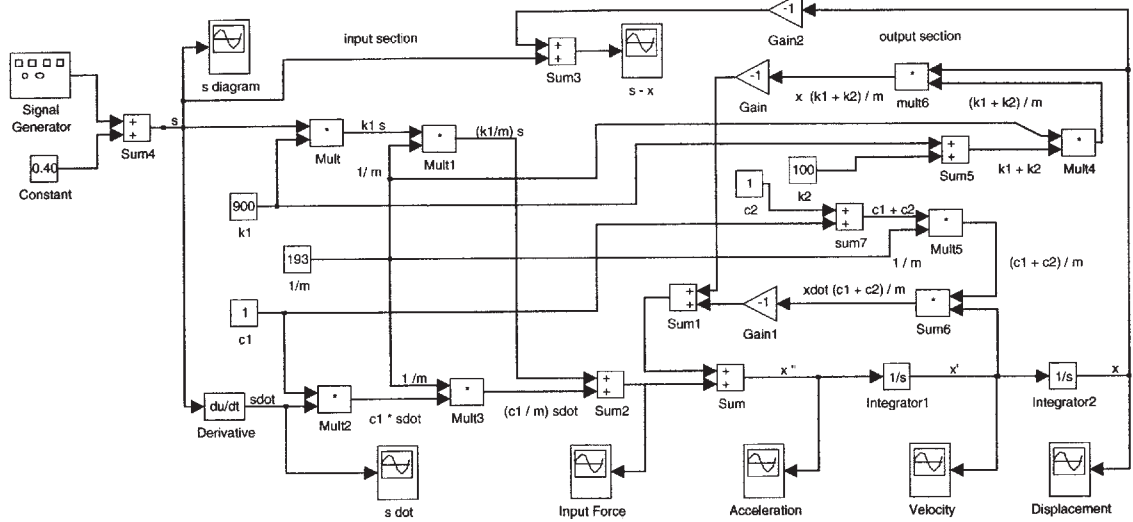
$$\ddot{x} = \frac{k_1}{m}s + \frac{c_1}{m}\dot{s} - \frac{c_1 + c_2}{m}\dot{x} - \frac{k_1 + k_2}{m}x \quad (10.13a)$$

$$\ddot{x} = \omega_1^2 s + 2\zeta_1 \omega_1 \dot{s} - 2\zeta_2 \omega_2 \dot{x} - \omega_2^2 x \quad (10.13b)$$

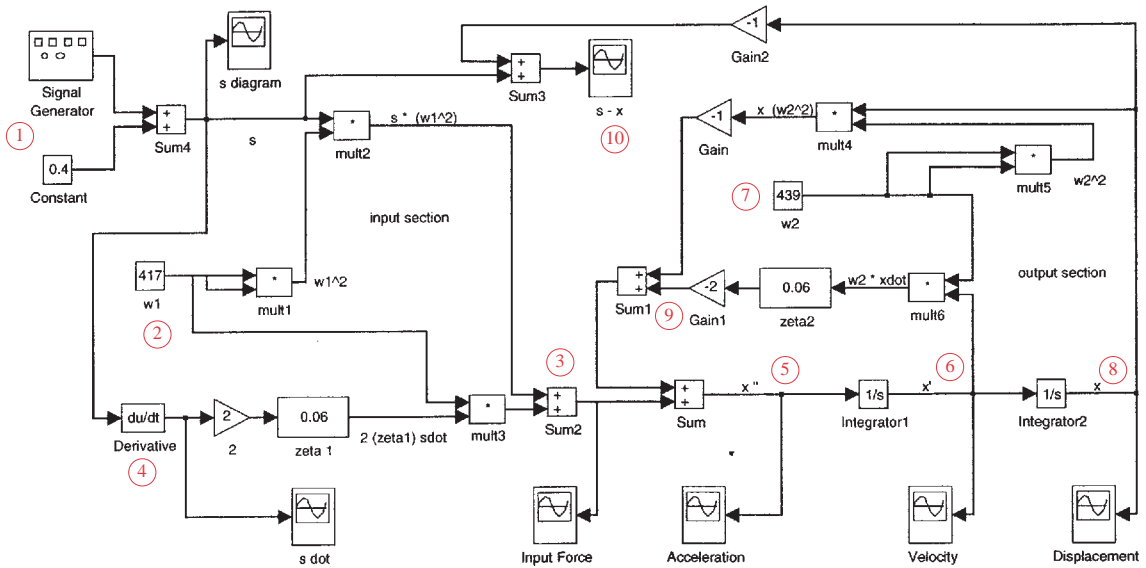
The first two terms on the right side of these equations are the input to the system, containing the designed cam displacement s and velocity $s\dot{}$.

Figure 10-13 shows two such block diagrams, created in SIMULINK. Figure 10-13a is a block diagram for equation 10-13a; it expresses the system motion in terms of the basic parameters m , k_1 , k_2 , c_1 , and c_2 . Figure 10-13b shows a block diagram for equation 10-13b; it defines the same system in terms of the natural frequencies ω_1 , ω_2 , and the dimensionless damping ratios ζ_1 and ζ_2 . If one wants to work in terms of the fundamental parameters of the system rather than normalized values, then Figure 10-13a would be preferred. Both models give identical results when solved numerically.

The block diagram for the normalized equation 10.13b in Figure 10-13b is somewhat "cleaner" and so is easier to follow. At point 1 (circled), a signal generator is used to provide an input function. This SIMULINK icon provides sine, sawtooth, square wave, and random noise functions. A different icon than shown allows the input of a tabulated function that can be the actual displacement and/or velocity data (including dwells) for the selected cam program, such as modified sine, cycloidal, or a custom spline program, for example.



(a) Block diagram for the solution of equation 10.13a (Simulink/Matlab)



(b) Block diagram for the solution of equation 10.13b (Simulink/Matlab)

FIGURE 10-13

Block diagrams for the solution of differential equation models of a cam-follower system

A constant is added to the sine wave in the *Sum4* block to force it positive for all values of time. In this simulation, the amplitude of the sine function for s is 0.25 in, and the offset is 0.4 in, making its displacement range from 0.15 to 0.65 in as shown in Figure 10-14a. The additional offset ($0.4 - 0.25 = 0.15$ in) acts to create the necessary spring preload on the system, defined as F_{pl} in equation 9.10 (p. 233).

This displacement s is fed to the *mult2* block where it is multiplied by ω_1^2 , which was created by multiplying the user-input value of ω_1 (point 2) by itself in the *mult1* block. This product is fed to the *sum2* block at point 3. The displacement s is also fed to the derivative block that creates \dot{s} (point 4), which is the second part of the input portion of equation 10.13b. Velocity \dot{s} is multiplied by a fixed gain of 2, then by an adjustable value for ζ_1 (using a graphical slider not shown). This product is then fed to *mult3* where it is multiplied by ω_1 to create the second term in equation 10.13b (p. 282), which is then added to the first term of the equation in block *sum2* at point 3. The output of *sum2* is fed to the block *sum* that combines it with the fed-back output from the calculation to create the value of \ddot{x} at point 5.

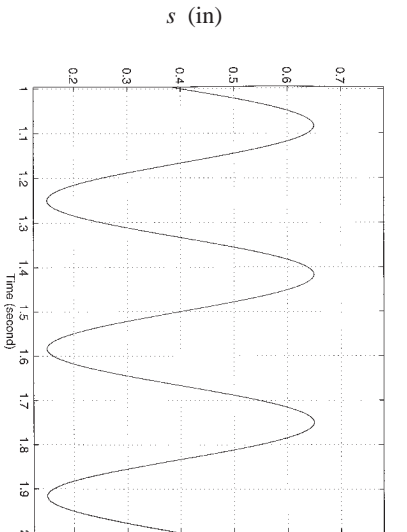
The value of \ddot{x} is passed through *integrator1* to create \dot{x} at point 6. This value is fed to block *mult6* to be multiplied by the value that was input for ω_2 at point 7. This result is multiplied by the selected value of ζ_2 and then by -2 to complete the third term of equation 10.13b at point 9.

The value of \dot{x} is passed through *integrator2* to create x (point 8), whose value is fed to block *mult4* where it is combined with ω_2^2 , and multiplied by -1 to create the fourth term in equation 10.13b (p. 282). This result is added to the third term of the equation in *sum1* at point 9. This result is fed into the block *sum* to be added to the input and close the loop to create \ddot{x} . An error function is created at point 10 by subtracting the calculated value of x from the input value of s .

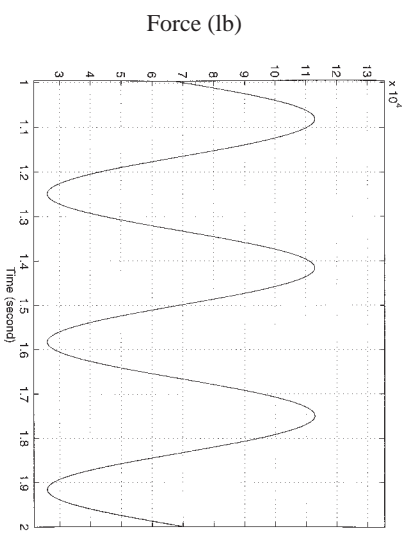
Several "storage scopes" are placed to display the values of the variables as the simulation proceeds. The simulation was run for 2 sec using an Adams integration algorithm. The input was a 3 Hz sine wave. Figure 10-14 shows the results for the period from 1 to 2 sec, after the initial transients have died out. Figure 10-14a shows the input displacement s . Figure 10-14b shows the cam-follower force that results. Figure 10-14c shows the output displacement x of the mass m . Figure 10-14d shows the error function ($s - x$). Figure 10-14e shows the velocity of the follower mass \dot{x} , which appears well behaved. Figure 10-14f shows the acceleration of the follower mass \ddot{x} , which shows considerable vibration activity. This reinforces the point made in the previous section that acceleration is the bellwether of vibration in dynamic systems. The MATLAB files for these examples are included on the attached CD-ROM.

Ordinary Differential Equation Solution—Using Mathcad

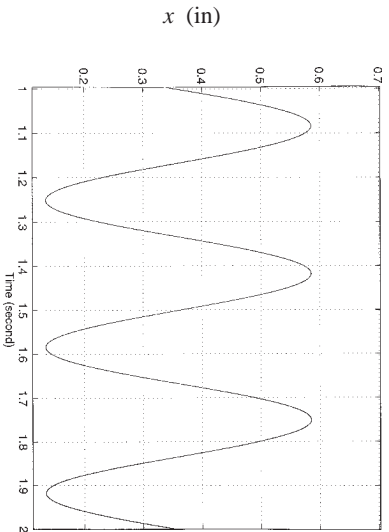
Mathcad 2000[®] has a very simple-to-use ODE solver. It is only necessary to write the ODE (of any order) as part of a "solve block" as shown in Figure 10-15. The equation can be expressed in implicit form as shown. Any parameters needed for its computation must be defined in *Mathcad* above the solve block. One such example is shown in the figure as a calculation of the natural frequency η_1 . The forcing functions $V_{pw}(t)$ and



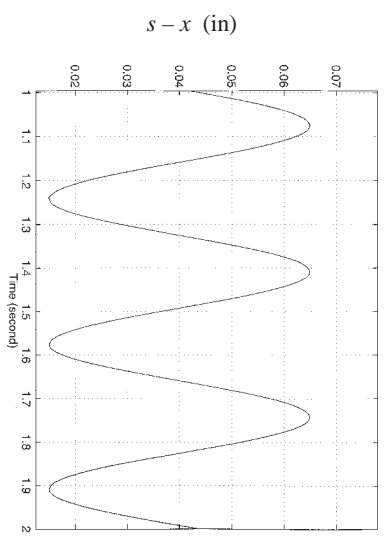
(a) Input cam displacement s



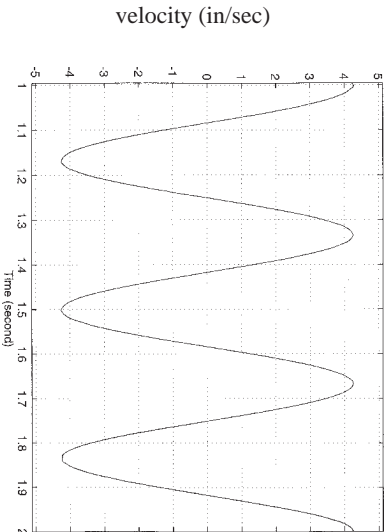
(b) Force between cam and follower



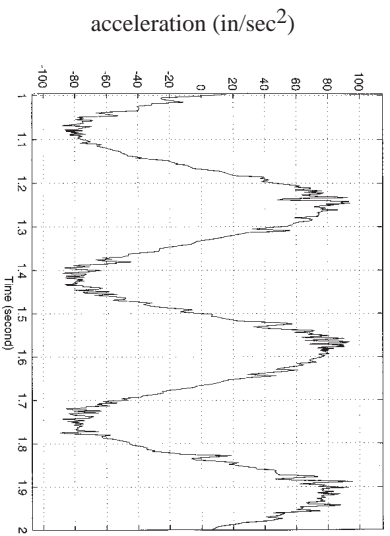
(c) Output displacement of follower x



(d) Error between input and output $s - x$



(e) Velocity of follower \dot{x}



(f) Acceleration of follower \ddot{x}

FIGURE 10-14

Steady-state solution to equation 10.13 for an arbitrary cam-follower system driven sinusoidally at 3 Hz

$$\eta_1 := \sqrt{\frac{k_{f01}}{m}}$$

The following solve block uses the Mathcad ODESOLVE function to solve for the follower response.

Given

$$\frac{d^2}{dt^2}x(t) + 2\zeta\eta_1\frac{d}{dt}x(t) + \eta_1^2x(t) = 2\zeta\eta_1V_{pw}(t)\frac{\omega}{1000} + \eta_1^2\frac{S_{pw}(t)}{1000}$$

$$x(0) = 0 \quad x'(0) = 0$$

$$R := \text{Odesolve}(t, t_{end}, inc_t)$$

FIGURE 10-15

Mathcad solve block to numerically integrate a differential equation

$S_{pw}(t)$, the forcing frequency ω , and the damping ratio ζ were all defined in the Mathcad file upstream of the solve block, but are not shown in Figure 10-15.

The two initial conditions needed for this second order ODE are then defined, here x and x' at time $t = 0$ are both set to zero. Then the built-in numerical solver ODESOLVE is called and passed values for start time t , end time, t_{end} , and a starting time increment inc_t . This solver uses a 4th-order Runge-Kutta algorithm with adaptive step size control and places the result in the variable R . The solution took only a few seconds to execute on a Pentium PC.

Figure 10-16 shows the result of the Mathcad solution to a cam-follower system run at 180 rpm with the following specifications: Dwell at 15 mm for 150°, modsine fall to zero in 45°, dwell at zero for 120°, and modsine rise to 15 mm in 45°. The follower effective mass is 10 kg, the return spring has $k_2 = 15\,000$ N/m and the follower train has $k_1 = 1\text{E}6$ N/m.

State Space Solutions

Most numerical ODE solver algorithms require that an ODE of order higher than one be converted to a set of simultaneous first-order ODE's for solution. This is called the *state space* form of the system equations. The solver algorithm is structured to do a single numerical integration of each equation in the set and iterate until it converges to a solution at each time step. Most solvers also implement a so-called *adaptive step size* algorithm. This allows it to take larger steps in regions where the functions are changing slowly and smaller steps where there is rapid change. This gives more accurate and quicker solutions. For a thorough discussion of the common ODE solver algorithms, see Press et al.^[21]

FORCE-CLOSED, ONE-MASS VALVE TRAIN MODEL To put a higher-order ODE into the state space configuration is a simple process. We will illustrate it first for the force-closed, single-mass system with its return spring at the end effector as shown in Figure 10-3a (p. 267). Its equation 10.1b is repeated here, rearranged and renumbered.

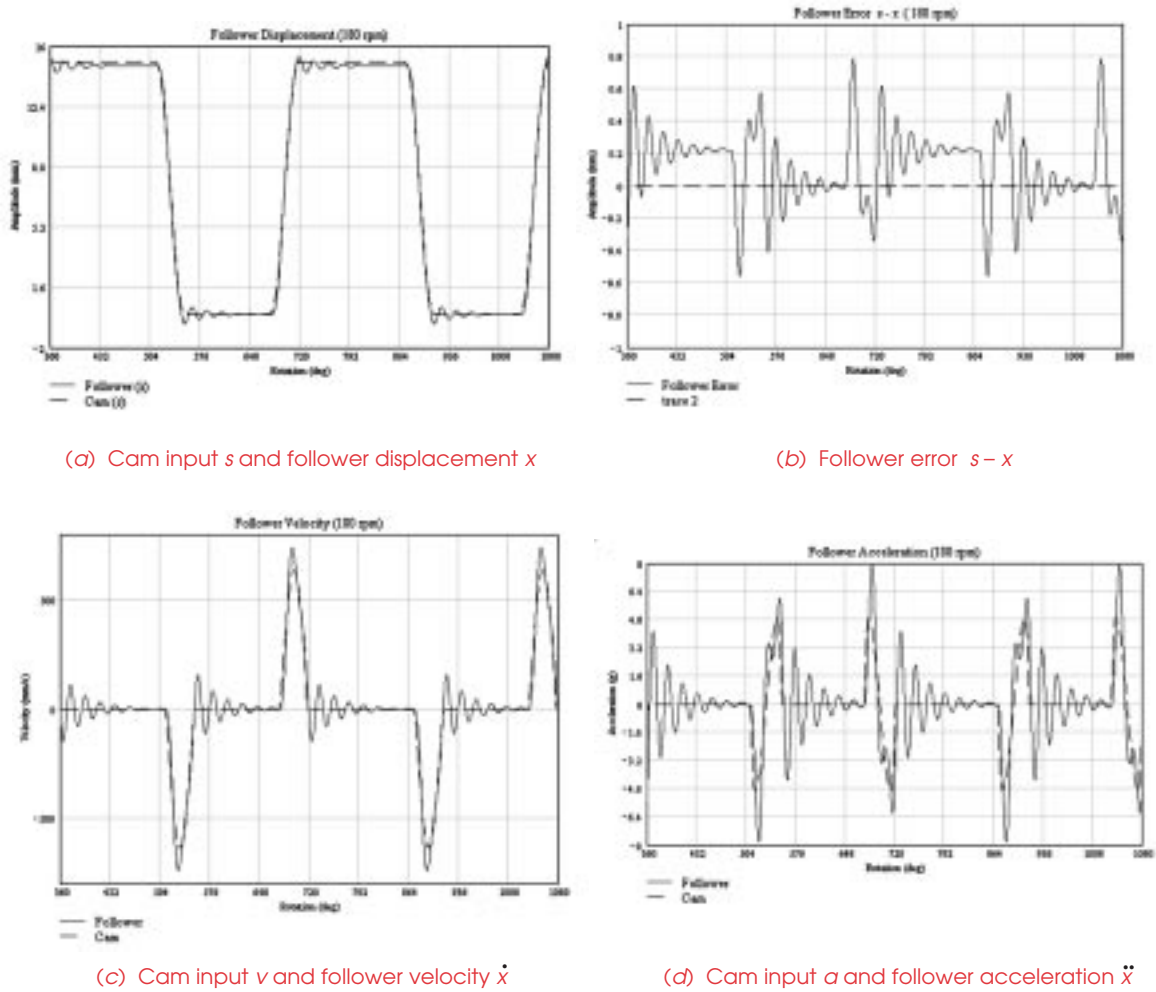


FIGURE 10-16

Mathcad solution to a cam-follower system modeled with equation 10.1 (Courtesy of Corey Maynard, of The Gillette Co.)

$$\ddot{x} = \omega_1^2 s + 2\zeta_1 \omega_1 \dot{s} - 2\zeta_2 \omega_2 \dot{x} - \omega_2^2 x \tag{10.14a}$$

First, create as many dummy variables as the order of the equation, here two, say y_1 and y_2 . Set one dummy variable to equal the independent variable, and one to equal its first derivative. (If the order were higher than 2, or there were more variables, then additional dummy variables would be needed).

$$y_1 = x \qquad y_2 = \dot{x} \tag{10.14b}$$

Now substitute the dummy variables into the original equation 10.14a to get:

$$\dot{y}_2 = \omega_1^2 s + 2\zeta_1 \omega_1 \dot{s} - 2\zeta_2 \omega_2 y_2 - \omega_2^2 y_1 \quad (10.14c)$$

This has reduced equation 10.14a to a first-order equation. The second equation is obtained by combining the dummy variable equations 10.14b. Together these comprise the state-space form of the system equations and can be solved simultaneously for y_1 and y_2 .

$$\dot{y}_1 = y_2 \quad (10.14d)$$

$$\dot{y}_2 = \omega_1^2 s + 2\zeta_1 \omega_1 \dot{s} - 2\zeta_2 \omega_2 y_2 - \omega_2^2 y_1$$

The results of their simultaneous solution are then back-substituted in the original equation 10.14a according to equation 10.14b and \ddot{x} computed.

FORM-CLOSED, ONE-MASS MODEL The form-closed system has no return spring and was modeled in Figure 10-8a (p.276). Its system equation 10.7b is repeated here, rearranged and renumbered.

$$\ddot{x} = \omega_n^2 s + 2\zeta \omega_n \dot{s} - 2\zeta \omega_n \dot{x} - \omega_n^2 x \quad (10.15a)$$

Establish two dummy variables as in equation 10.14b and create two coupled first-order state space ODEs for solution.

$$\dot{y}_1 = y_2 \quad (10.15b)$$

$$\dot{y}_2 = \omega_n^2 s + 2\zeta \omega_n \dot{s} - 2\zeta \omega_n y_2 - \omega_n^2 y_1$$

The results of their simultaneous solution are then back-substituted in the original equation 10.15a according to equation 10.14b and \ddot{x} computed.

FORCE-CLOSED, ONE-MASS INDUSTRIAL CAM MODEL The one-mass, force-closed system with its return spring at the cam was modeled in Figure 10-8b. Its system equation 10.8b for the in-contact condition is repeated here, rearranged and renumbered.

$$\ddot{x} = \omega_2^2 s + 2\zeta_2 \omega_2 \dot{s} - 2\zeta_2 \omega_2 \dot{x} - \omega_2^2 x \quad (10.16a)$$

Establish two dummy variables as in equation 10.14b and create two coupled first-order state space ODEs for solution.

$$\dot{y}_1 = y_2 \quad (10.16b)$$

$$\dot{y}_2 = \omega_2^2 s + 2\zeta_2 \omega_2 \dot{s} - 2\zeta_2 \omega_2 y_2 - \omega_2^2 y_1$$

The results of their simultaneous solution are then back-substituted in the original equation 10.16a according to equation 10.14b and \ddot{x} computed.

FORCE-CLOSED, TWO-MASS INDUSTRIAL CAM MODEL The two-mass force-closed system with its return spring at the cam was modeled in Figure 10-11 (p. 279). Its system equation 10.12a for the in-contact condition is repeated and renumbered here.

$$\ddot{x} = \frac{c_2}{m_2} \dot{z} + \frac{k_2}{m_2} z - \frac{c_2}{m_2} \dot{x} - \frac{k_2}{m_2} x \quad (10.17a)$$

Establish two dummy variables as in equation 10.14b and create two coupled first-order state space ODEs for solution.

$$\begin{aligned} \dot{y}_1 &= y_2 \\ \dot{y}_2 &= \frac{c_2}{m_2} \dot{z} + \frac{k_2}{m_2} z - \frac{c_2}{m_2} y_2 - \frac{k_2}{m_2} y_1 \end{aligned} \quad (10.17b)$$

As described in the previous section, this equation only covers the case of contact between cam and follower (stage 1). It is solved assuming that the displacement z of m_1 equals cam displacement s for a given time step. Then the contact force F_c is calculated from equation 10.12b using the values of x and its derivatives found from equations 10.17b. If F_c is positive, then equations 10.17b are used again at the next time step. If F_c becomes negative, then separation has occurred and the solution must switch to stage 2, which requires simultaneous solution of equations 10.12a and 10.12b for x and z with F_c set to zero and the initial conditions set to the current values of position and velocity.

$$\begin{aligned} \ddot{x} &= \frac{c_2}{m_2} \dot{z} + \frac{k_2}{m_2} z - \frac{c_2}{m_2} \dot{x} - \frac{k_2}{m_2} x \\ \ddot{z} &= -\frac{c_1 + c_2}{m_1} \dot{z} - \frac{k_1 + k_2}{m_1} z + \frac{c_2}{m_1} \dot{x} + \frac{k_2}{m_1} x \end{aligned} \quad (10.17c)$$

These two second-order ODEs require four dummy variables.

$$y_1 = x \quad y_2 = \dot{x} \quad y_3 = z \quad y_4 = \dot{z} \quad (10.17d)$$

Substitution of equation 10.17d into 10.17c leads to the following set of state space equations.

$$\begin{aligned} \dot{y}_1 &= y_2 \\ \dot{y}_2 &= \frac{c_2}{m_2} y_4 + \frac{k_2}{m_2} y_3 - \frac{c_2}{m_2} y_2 - \frac{k_2}{m_2} y_1 \\ \dot{y}_3 &= y_4 \\ \dot{y}_4 &= -\frac{c_1 + c_2}{m_1} y_4 - \frac{k_1 + k_2}{m_1} y_3 + \frac{c_2}{m_1} y_2 + \frac{k_2}{m_1} y_1 \end{aligned} \quad (10.17e)$$

These equations are solved, and their values of x and z used in equation 10.12b, to determine F_c . As long as F_c continues to be negative, this stage 2 solution is continued. When F_c goes positive, the solution is switched back to equations 10.17b. Another possibility is to compare the calculated value of z to the cam displacement s at each time step in stage 2 to determine when z again becomes equal to or less than s , indicating that contact has been reestablished.

IMPLEMENTATION This state-space approach has been implemented in program DYNACAM and can be solved for any of these five models (equations 10.5c-d, 10.8, 10.14, 10.15, 10.16, or 10.17).^{*} It uses a fourth-order Runge-Kutta algorithm with adaptive step size control. A typical solution screen (for equation 10.14) is shown in Figure

* For the two-mass cam models as defined in equations 10.5c-d, and 10.17, program Dynacam only solves equations 10.17b and calculates the dynamic force from equation 10.12b. If the force goes negative, it records the angle at which that occurred and thereafter ceases to calculate the force. The system parameters can be changed to eliminate follower jump and the system dynamics recalculated.

10-17. The system parameters (m , k_1 , k_2 , ζ_1 , ζ_2) are supplied by the user. The natural frequencies ω_1 and ω_2 are calculated from the m - k data to be used in the solution. The user can also specify the desired start and end times for the calculation and the initial value of displacement (initial velocity is assumed to be zero). The starting time step, end time, minimum step size, and accuracy are also user controllable, though good results will be obtained by accepting their default values. The end time is required to be at least two cam rotation periods in order to let the starting transients die out. The data plotted from DYNACAM's plot routines shows one cam revolution cycle, beginning with the second revolution, in order to eliminate the transient effects.

The example shown in Figure 10-17 is of a double-dwell cam having a modified-trapezoidal acceleration rise of 1 in over 90° , a 90° dwell, a 90° modified-sine acceleration fall, and a 90° dwell. Camshaft speed is 180 rpm. Compare the simulated acceleration of the modified trapezoidal rise with that of Figure 9-10 (p. 232), which shows a measurement of the acceleration of a similar cam-follower program. They are quite similar.

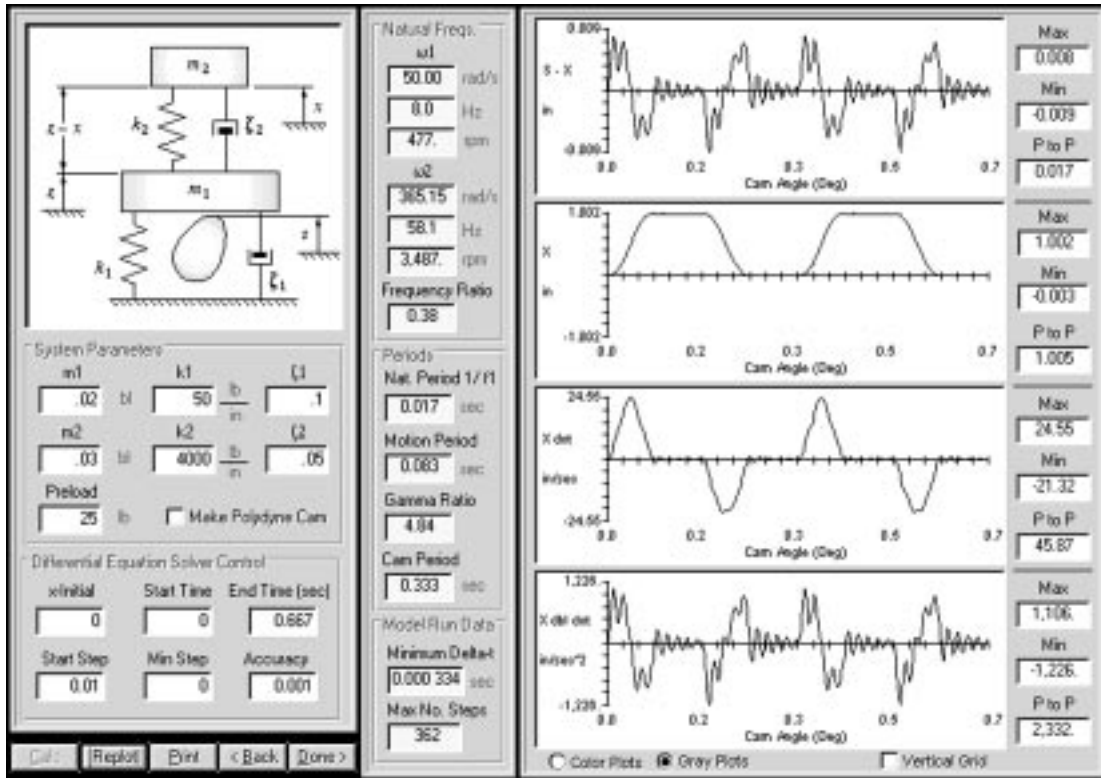


FIGURE 10-17

Dynamic model input and calculation in program DYNACAM

10.8 POLYDYNE CAM FUNCTIONS

The term polydyne is a contraction of "polynomial" and "dynamic." It was coined by Thoren, Engemann, and Stoddart in 1953^[12] to describe a cam design method first proposed and implemented by Dudley in 1948,^[13] who was the first to use a dynamic model of a cam-follower system such as those described in the previous sections of this chapter to determine a cam profile that would, in effect, compensate for the dynamic vibration of the follower train, at least at one particular cam speed. Dudley used a simple SDOF model that did not include damping, as shown in Figure 10-18. The equation of motion for this system is:

$$\begin{aligned} m\ddot{x} &= k_1(s - x) - k_2x \\ &= k_1s - (k_1 + k_2)x \end{aligned} \quad (10.18a)$$

This equation relates the cam displacement s to the follower displacement x . In the previous sections, we defined the cam displacement s and solved for x . However, the equation works in the other direction as well. We can define the desired follower motion x and its derivatives and compute the cam displacement s needed to obtain that displacement with the assumed spring rates and known mass of the system. Solving equation 10.18a for s gives:

$$s = \frac{m}{k_1} \ddot{x} + \frac{k_1 + k_2}{k_1} x \quad (10.18b)$$

The acceleration \ddot{x} has units of length/sec². It will be useful to convert it to an angle base (in degrees) rather than a time base and to introduce the camshaft angular velocity N in rpm.

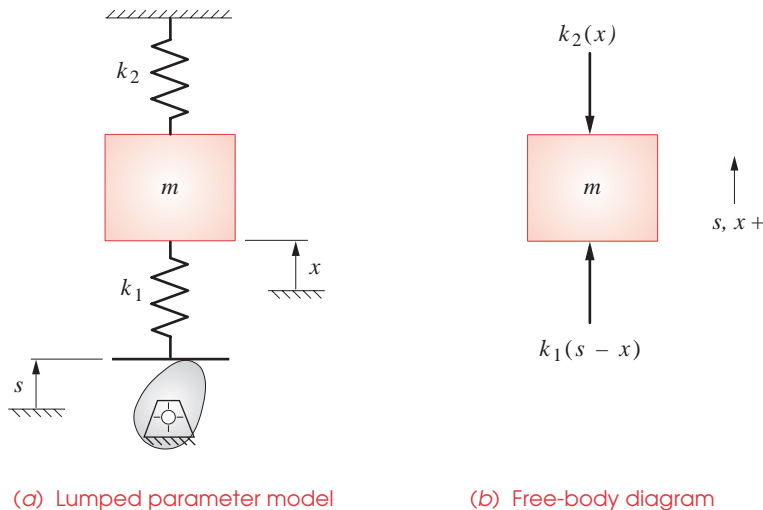


FIGURE 10-18

Dudley's SDOF model and FBD of a cam-follower system for a polydyne cam ^[13]

$$\frac{\text{length}}{\text{sec}^2} = \frac{\text{length}}{\text{deg}^2} \left(\frac{360^2 \text{ deg}^2}{\text{rev}^2} \right) \left(\frac{N^2 \text{ rev}^2}{60^2 \text{ sec}^2} \right)$$

$$\ddot{x} = \frac{d^2 x}{dt^2} = 36N^2 \frac{d^2 x}{d\theta^2} \quad (10.19)$$

Substitute equation 10.19 in 10.18b.

$$s = \left(36N^2 \frac{m}{k_1} \right) \frac{d^2 x}{d\theta^2} + \left(\frac{k_1 + k_2}{k_1} \right) x \quad (10.20a)$$

Differentiate with respect to θ to get the polydyne cam velocity function.

$$\dot{s} = \left(36N^2 \frac{m}{k_1} \right) \frac{d^3 x}{d\theta^3} + \left(\frac{k_1 + k_2}{k_1} \right) \frac{dx}{d\theta} \quad (10.20b)$$

Differentiate again with respect to θ to get the polydyne cam acceleration function.

$$\ddot{s} = \left(36N^2 \frac{m}{k_1} \right) \frac{d^4 x}{d\theta^4} + \left(\frac{k_1 + k_2}{k_1} \right) \frac{d^2 x}{d\theta^2} \quad (10.20c)$$

Note that the cam acceleration function involves the fourth derivative of the selected follower displacement function, which we call "ping." This means that any function selected for the follower displacement must be continuous through at least four derivatives, velocity, acceleration, jerk, and ping. Since polynomial functions allow control of continuity at the ends of the segment to any derivative, they provide a useful means to this end. Spline functions can also satisfy these requirements.

Dudley's polydyne model of Figure 10-18 is for a system with the return spring acting at the end effector. For an industrial cam that has the return spring acting on the cam shoe, the model of Figure 10-8 is more appropriate. If we assume that contact is maintained between cam and follower and that damping is negligible, we can write the system equation as a modification of equation 10.7, leaving out the damping terms.

$$\ddot{x} + \frac{k}{m} x = \frac{k}{m} s \quad (10.21a)$$

Rearrange to solve for s :

$$s = \frac{m}{k} \ddot{x} + x \quad (10.21b)$$

Substitute equation 10.19 in 10.21b

$$s = 36N^2 \frac{m}{k} \frac{d^2 x}{d\theta^2} + x \quad (10.22a)$$

Differentiate with respect to θ to get the polydyne cam velocity function.

$$\dot{s} = 36N^2 \frac{m}{k} \frac{d^3 x}{d\theta^3} + \frac{dx}{d\theta} \quad (10.22b)$$

Differentiate again with respect to θ to get the polydyne cam acceleration function.

$$\ddot{s} = 36N^2 \frac{m}{k} \frac{d^4 x}{d\theta^4} + \frac{d^2 x}{d\theta^2} \quad (10.22c)$$

Note the presence of cam speed N in equations 10.20 and 10.22. For any selected follower function x and its derivatives, the cam profile, as defined by the function s (equation 10.20a or 10.22a) will be different for any value of N selected. This means that the dynamic behavior of the system can be optimized (i.e., vibration minimized) only for one operating speed. If the system will be operated at a single speed, this is not a problem. If not, then one speed in its range will have to be selected for the cam profile definition and the system will have some vibration when operated at any other speed. When applied to engine valve trains that obviously operate over a wide range of speeds, a speed close to the highest expected operating speed is typically used in equations 10.20. Fawcett and Fawcett^[20] show that a polydyne cam will always give lower vibration than a non-polydyne cam having the same follower program when its speed is greater than $0.707N$. They also state that:

By a suitable choice of N , the speeds at which a polydyne cam is inferior may be relegated to the lower part of the speed range of the mechanism where (the inherently lower, ed.) vibration amplitudes are not a problem.

Given an effective dynamic model of the system as described by equation 10.18a, the problem devolves to identifying one or more suitable polynomial functions for x that provide sufficient control of continuity and that also yield acceptable peak values of velocity and acceleration of the follower for any given set of kinematic constraints on the follower motion. However, Dudley points out that:

With a flexible valve linkage, one must accept higher accelerations at the valve (follower) than would occur with a rigid connecting system. There is a corollary: If a cam is designed on the assumption of a rigid system, the actual limiting speed will be appreciably lower than the theoretical value.

The derivations of these polydyne polynomials are long and involved and will not be reproduced here. The interested reader can explore them in the original references given. Dudley addressed the problem of valve cam design for the overhead valve-pushrod cam-follower system as shown in Figure 10-1, which is a relatively soft system and can have significant vibration problems. In valve trains, it also is necessary to maximize the area under the valve lift curve since it directly affects engine breathing. Dudley included this constraint in his development of the equations. He also attempted to minimize peak accelerations and to have an acceleration curve not dissimilar in shape to those that had proven successful in the past. Some trial and error was involved, particularly in respect to choice of powers to be used in the x equation. He determined that a polynomial equation of this form was suitable.

$$s = h \left[1 + C_2 \left(\frac{\theta}{\beta} \right)^2 + C_p \left(\frac{\theta}{\beta} \right)^p + C_q \left(\frac{\theta}{\beta} \right)^{p+2} + C_r \left(\frac{\theta}{\beta} \right)^{p+4} \right] \quad (10.23a)$$

where the constants are defined by:

$$C_2 = \frac{-6p^2 - 24p}{6p^2 - 8p - 8} \quad (10.23b)$$

$$C_p = \frac{p^3 + 7p^2 + 14p + 8}{6p^2 - 8p - 8} \quad (10.23c)$$

$$C_q = \frac{-2p^3 - 4p^2 + 16p}{6p^2 - 8p - 8} \quad (10.23d)$$

$$C_r = \frac{p^3 - 3p^2 + 2p}{6p^2 - 8p - 8} \quad (10.23e)$$

He comments that "retaining the power 2 provides nearly constant acceleration in the center of the curve, and increasing the exponents of the other three terms has the effect of moving the inflection point further out." This leads to a set of polynomials with exponents of 2-4-6-8, 2-6-8-10, 2-8-10-12, 2-10-12-14, and 2-12-14-16. Of these, Dudley claims "the 2-10-12-14 is probably the best." Its equation is:

$$s = \frac{h}{64} \left[64 - 105 \left(\frac{\theta}{\beta} \right)^2 + 231 \left(\frac{\theta}{\beta} \right)^{10} - 280 \left(\frac{\theta}{\beta} \right)^{12} + 90 \left(\frac{\theta}{\beta} \right)^{14} \right] \quad (10.24)$$

The lift curve and its first four derivatives are shown in Figure 10-19. Equations 10.23 define only the fall portion of the RFD function. The rise is a mirror image of the fall, switched left to right. To calculate the rise, the independent variable θ/β must be run backward from 1 to 0, and then the velocity and jerk functions must be negated as well. Note in Figure 10-19 that the jerk is discontinuous at the dwells, violating the rule stated by Dudley for functions to be used for polynomial cams (see the discussion of equation 10.20 on p. 292).

Thoren, Engemann, and Stoddart also developed other polynomials for the pushrod overhead valve train that used higher powers than Dudley's and that are continuous in all derivatives through ping.^[12] They define a 6-term polynomial of the form

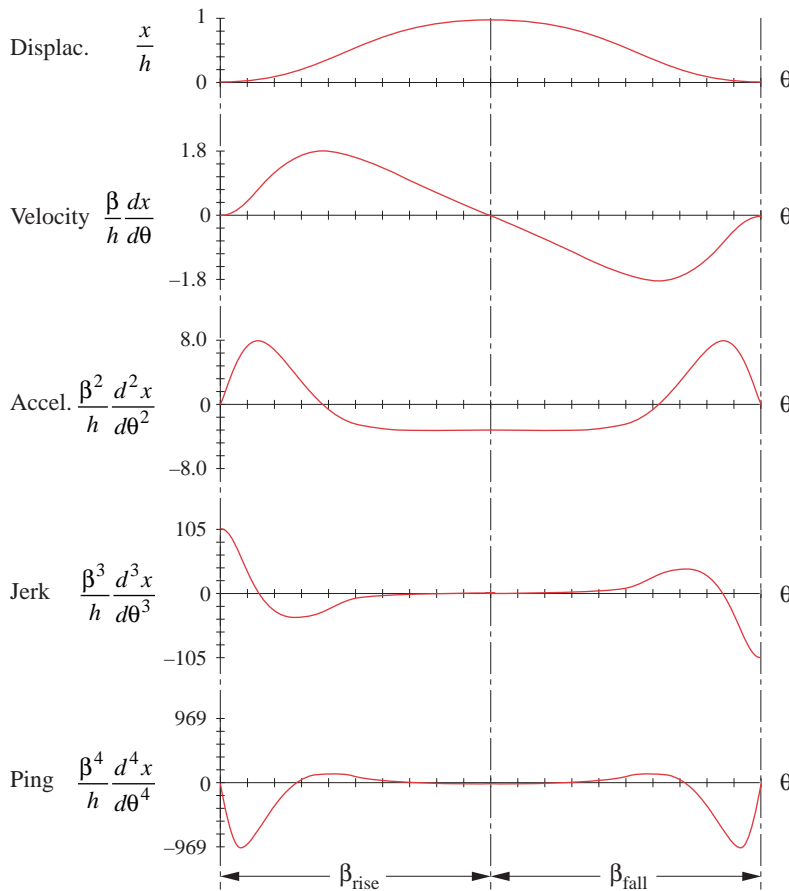
$$s = h \left[1 + C_2 \left(\frac{\theta}{\beta} \right)^2 + C_p \left(\frac{\theta}{\beta} \right)^p + C_q \left(\frac{\theta}{\beta} \right)^q + C_r \left(\frac{\theta}{\beta} \right)^r + C_s \left(\frac{\theta}{\beta} \right)^s \right] \quad (10.25a)$$

where the constants are defined by:

$$C_2 = \frac{-pqrs}{(p-2)(q-2)(r-2)(s-2)} \quad (10.25b)$$

$$C_p = \frac{2qrs}{(p-2)(q-p)(r-p)(s-p)} \quad (10.25c)$$

$$C_q = \frac{-2prs}{(q-2)(q-p)(r-q)(s-q)} \quad (10.25d)$$


FIGURE 10-19

A 2-10-12-14 polynomial rise-return follower function for a polydyne valve cam

$$C_r = \frac{2pqs}{(r-2)(r-p)(r-q)(s-r)} \quad (10.25e)$$

$$C_s = \frac{-2pqr}{(s-2)(s-p)(s-q)(s-r)} \quad (10.25f)$$

They used evenly spaced exponent sets, i.e., $q - p = r - q = s - r$. Figure 10-20 shows the follower functions for a 2-10-20-30-40 polynomial, and Figure 10-21 shows a 2-14-26-38-50 polynomial. These plots are normalized to show dimensionless factors for their peak values. Note that the higher-order polynomial (Figure 10-21) has significantly higher peak acceleration than the one in Figure 10-20 (13.2 vs. 10.4), but also has a smaller negative acceleration (-2.8 vs. -3.1) because of the steeper and shorter positive acceleration pulses. Less negative acceleration requires less spring force to keep the follower in contact with the cam, which can be an advantage.

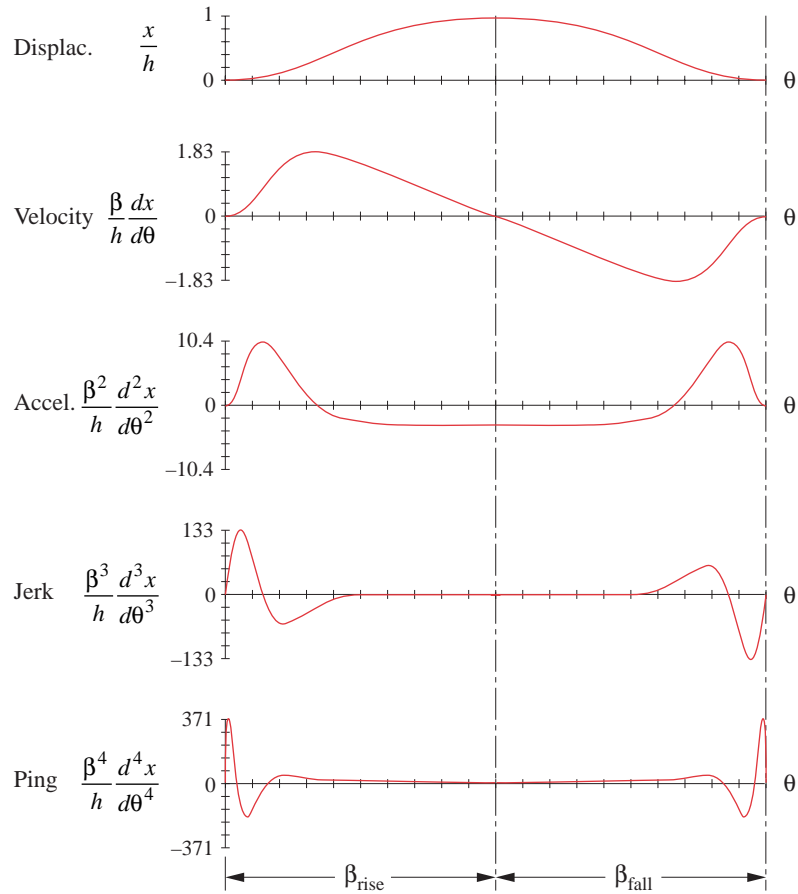


FIGURE 10-20

A 2-10-20-30-40 polynomial rise-return follower function for a polydyne valve cam

Figure 10-22 (p. 298) shows both the cam and the follower curves for displacement, velocity, and acceleration for a 2-10-20-30-40 polynomial on the rise and a 2-10-16-24-30 polynomial on the fall from [16]. Note that the cam displacement s is larger than the valve displacement x over the entire motion, indicating that the "spring" in the system is "wound up" during the entire event. Recognize that the cam is cut to the solid curve, but the follower takes the dotted path. The velocity of the valve is greater than that of the cam function at its peaks. The acceleration curves show the greatest differences. Note how the cam acceleration curve dips to nearly zero at the beginning of the rise to compensate for the tendency of the valve acceleration to overshoot. A similar but smaller difference is seen near the end of the fall.

Stoddart [14], [15], [16] continued Dudley's work on polydyne cams for valve trains and developed a characteristic relationship of vibration amplitude versus cam speed as shown in Figure 10-23 (p. 299). The actual amplitude A of this curve will vary with the partic-

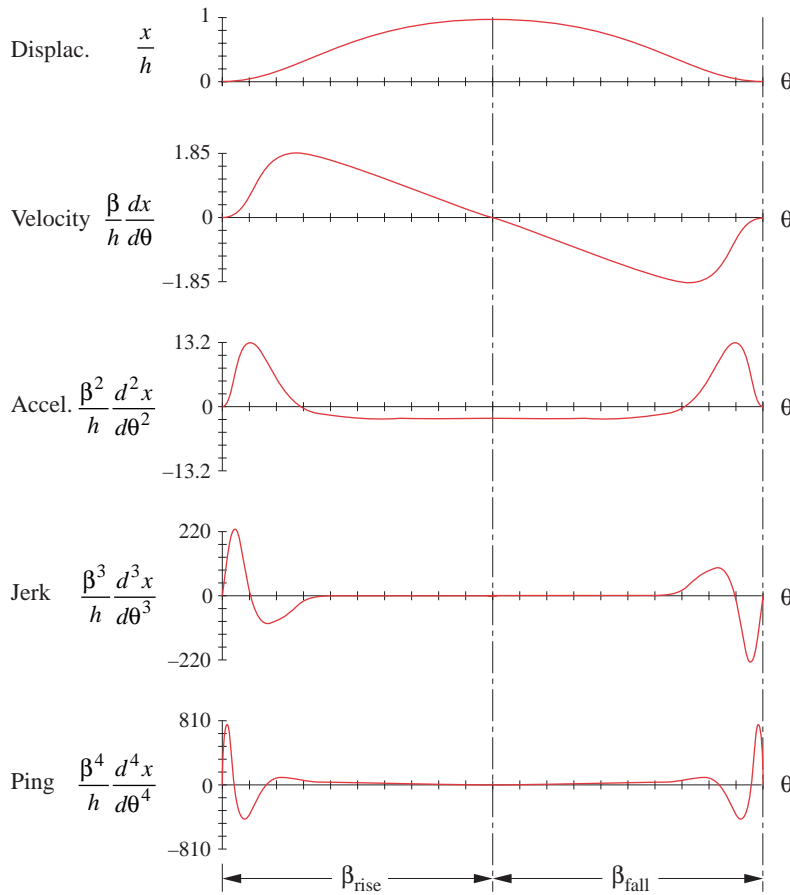
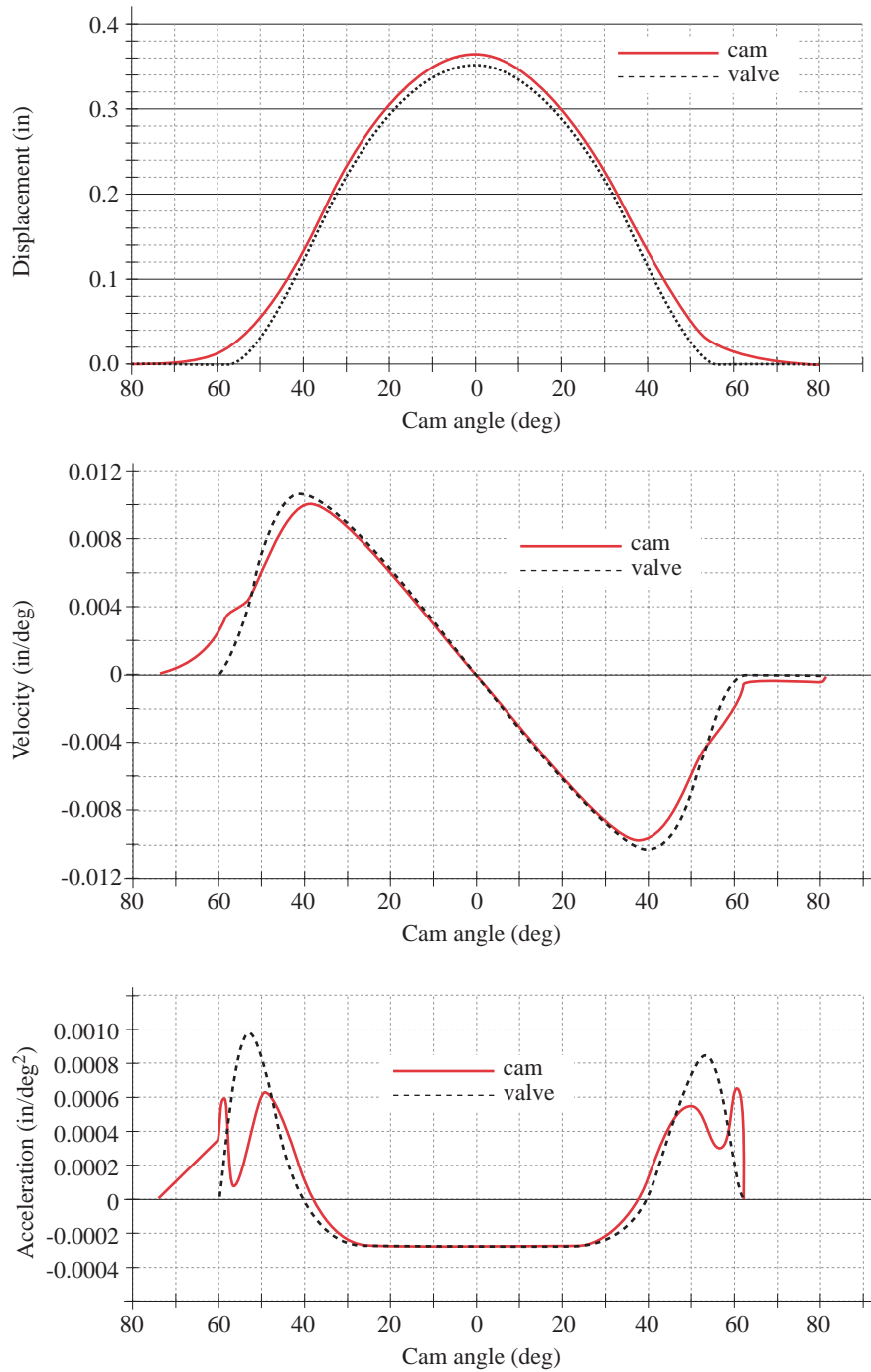


FIGURE 10-21

A 2-14-26-38-50 polynomial rise-return follower function for a polydyne valve cam

ular follower train, but the shape will be similar in all cases. The sign of A is not of interest since the direction of vibration is not relevant, only its magnitude. Note that the vibration amplitude is zero at the design speed N , peaks at $0.707N$, and reaches the same level A at $1.1N$, increasing rapidly at higher speeds.

Polydyne functions were used extensively for automotive valve cams in the U. S. in the 1950's and 1960's, but they have not been used in these applications in recent years. Instead, spline functions are now more commonly used for valve trains. Figure 10-24 shows a modern spline-function design for a single overhead camshaft (SOHC) valve train.^[17] Note the asymmetry of the acceleration function, a design freedom allowed by the use of spline functions. This design uses a quartic spline for displacement, but is designed from the acceleration using designer-shaped quadratic splines.^[18] The step functions in the acceleration function before and after the lift event are the opening and closing ramps used to wind up the system compliance.^[17]

**FIGURE 10-22**

Cam and follower (valve) motions with a polydyne cam (14, 15, 16)

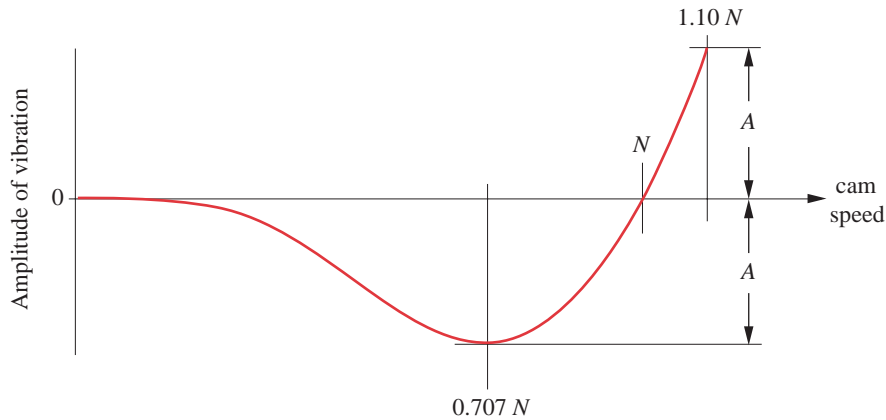


FIGURE 10-23

Characteristic relationship of vibration with cam speed for polydyne cams (14, 15, 16)

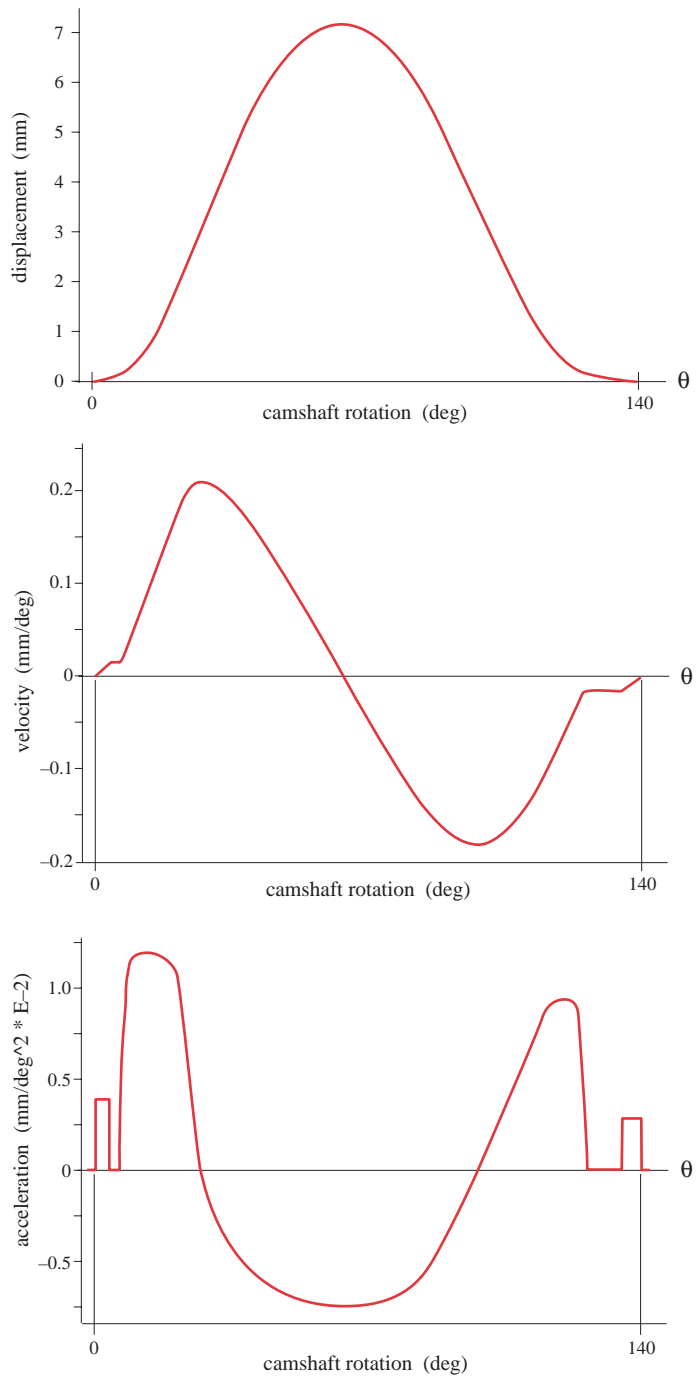
The abandonment of polydyne cams by most automobile engine manufacturers was due mainly to the inherent limitation of the polydyne method to one cam speed. Also, the current trend in engine design is to overhead camshaft valve trains as shown in Figure 10-25 (p. 301), rather than the pushrod-overhead valve train type shown in Figure 10-1 (p. 265). The former have much shorter and stiffer follower trains than the latter and so do not exhibit as much variation in dynamic motion between cam and valve. Current valve cam design uses very sophisticated multi-DOF dynamic models of the valve train (analogous to Seidlitz's model) that contain accurate representations of the hydraulic lash adjuster's nonlinear behavior as well as multi-DOF models of the valve spring. Computer programs written specifically to simulate the dynamic behavior of valve trains are commercially available.*

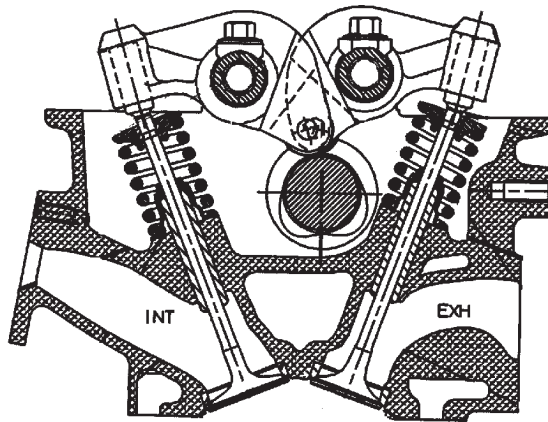
Double-Dwell Polydyne Curves

Polydyne cams were first developed for the single-dwell automobile engine valve train but others have adapted the technique to double-dwell machine cams as well. Stoddart^[14] shows how to develop double-dwell polynomials suitable for a polydyne application but does not appear to provide a viable solution in reference [14]. Peisekah^[19] derives a useful solution to this problem. He uses the same model as Dudley (Figure 10-18 on p. 291) and its system equation 10.18 (p. 291) to define follower motion. The polydyne cam displacement function and its derivatives are as shown in equation 10.20 (p. 292). As these equations show, the chosen follower function $x(\theta)$ should be continuous through the fourth derivative of displacement or ping. For a double-dwell motion with a total rise of h and a normalized independent variable $u = \theta/\beta$, this requires the minimum set of boundary conditions (BCs):

$$\begin{aligned}
 &\text{when } u = 0, & x &= 0 & x' &= 0 & x'' &= 0 & x''' &= 0 & x'''' &= 0 \\
 &\text{when } u = 1, & x &= h & x' &= 0 & x'' &= 0 & x''' &= 0 & x'''' &= 0
 \end{aligned}
 \tag{10.26}$$

* e.g., *Valdyne*, available from Ricardo, Bridge Works, Shoreham-by-Sea, West Sussex BN43 5FG England U.K.

**FIGURE 10-24**Spline functions for follower motion of a SOHC valve train ⁽¹⁷⁾

**FIGURE 10-25**

Single overhead camshaft valve train (Courtesy of DaimlerChrysler, Auburn Hills, MI)

These 10 BCs will yield the 9th-degree polynomial

$$x = h[126u^5 - 420u^6 + 540u^7 - 315u^8 + 70u^9] \quad (10.27)$$

Unfortunately, this function's second derivative has a maximum acceleration factor of $9.37 h/\beta^2$, which is rather high compared to the standard double-dwell functions shown in Table 3-2 (p. 50).

Peisekah^[19] added two additional BCs to derive an 11th-degree polynomial as shown in Figure 10-26. One of the additional BCs was used to force symmetry by making $x(0.5) = 0.5h$. The remaining BC was used as a free variable, and iterated to minimize the value of peak acceleration. The resulting function is:

$$x = h \begin{bmatrix} 336u^5 - 1890u^6 + 4740u^7 - 6615u^8 \\ +5320u^9 - 2310u^{10} + 420u^{11} \end{bmatrix} \quad (10.28a)$$

$$x' = h \begin{bmatrix} 1680u^4 - 11340u^5 + 33180u^6 - 52920u^7 \\ +47880u^8 - 23100u^9 + 4620u^{10} \end{bmatrix} \quad (10.28b)$$

$$x'' = h \begin{bmatrix} 6720u^3 - 56700u^4 + 199080u^5 - 370440u^6 \\ +383040u^7 - 207900u^8 + 46200u^9 \end{bmatrix} \quad (10.28c)$$

$$x''' = \frac{h}{\beta^3} \begin{bmatrix} 20160u^2 - 226800u^3 + 995400u^4 - 222640u^5 \\ +2681280u^6 - 1663200u^7 + 415800u^8 \end{bmatrix} \quad (10.28d)$$

This polynomial function has a maximum theoretical acceleration factor of $7.91 h/\beta^2$, which, though still high compared to the functions in Table 3-2 (p. 50), may be ac-

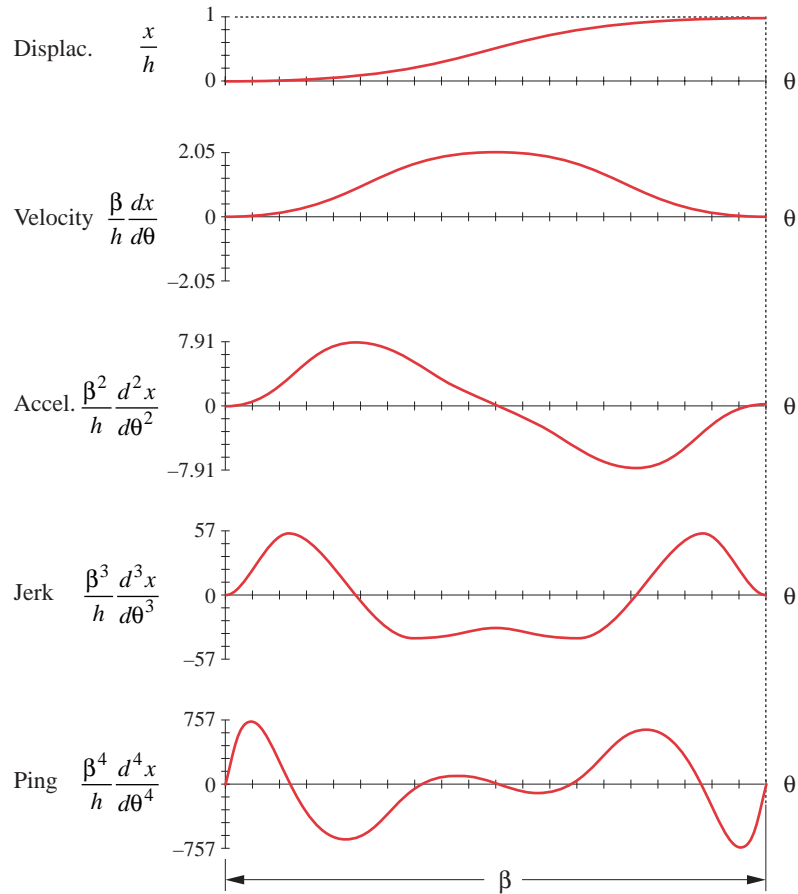


FIGURE 10-26

A Peisekah 5-6-7-8-9-10-11 polynomial rise-return follower function for a polydyne cam⁽¹⁹⁾

ceptable when the reduction of vibration at the design speed achieved by the polydyne method is taken into account as is shown in the following example.

EXAMPLE 10-1

Designing a Polydyne Double-Dwell Cam With Closure Spring at End Effector.

Problem: Consider the following statement of a double-dwell motion problem:

| | |
|--------------|---------------------|
| Rise | 1 in over 100° |
| Dwell | for 80° |
| Fall | 1 in over 100° |
| Dwell | for 80° |
| Speed | 425 rpm (7.083 Hz) |
| m_{eff} | 0.0104 blob* (4 lb) |

* See Section 1.6, p. 10

- k_1 1 000 lb/in for the linkage
- k_2 50 lb/in at the end effector
- Preload 25 lb
- ζ_1, ζ_2 0.05

Assumptions: The joint closure spring is at the end effector, so a SDOF, one-mass model as shown in Figure 10-2a (p. 266) will be used.

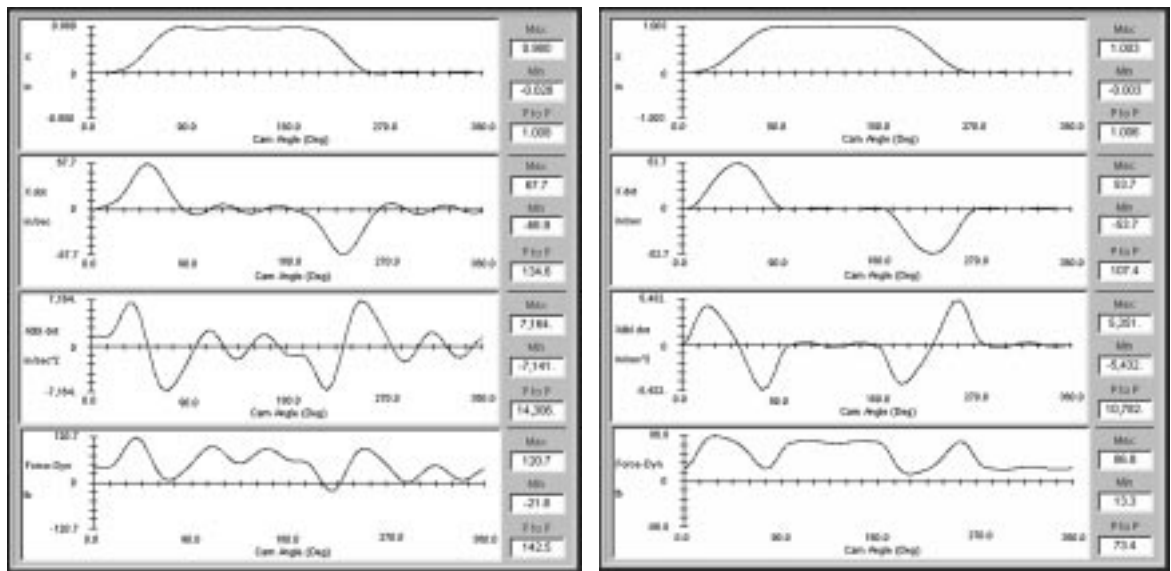
Solution:

- 1 A polydyne function theoretically requires continuity through ping, so a Peisekah polynomial will be used as defined in equations 10.28. Calculate the theoretical kinematic *SVAJP* functions for this design. The peak kinematic acceleration is 5143 in/sec².
- 2 Create the differential equation of the system using the relevant effective mass and spring constants based on equation 10.13b (p. 282).

$$\ddot{x} = \omega_1^2 s + 2\zeta_1 \omega_1 \dot{s} - 2\zeta_2 \omega_2 \dot{x} - \omega_2^2 x$$

$$\ddot{x} = \frac{k_1}{m} s + 2\zeta_1 \sqrt{\frac{k_1}{m}} \dot{s} - 2\zeta_2 \sqrt{\frac{k_1 + k_2}{m}} \dot{x} - \frac{k_1 + k_2}{m} x$$

$$\ddot{x} = \frac{1000}{0.0104} s + 2(0.05) \sqrt{\frac{1000}{0.0104}} \dot{s} - 2(0.05) \sqrt{\frac{1050}{0.0104}} \dot{x} - \frac{1050}{0.0104} x \quad (a)$$



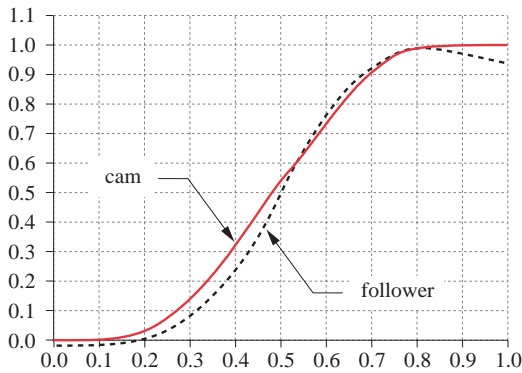
(a) Dynamic response of a nonpolydyne cam

(b) Dynamic response of a polydyne cam

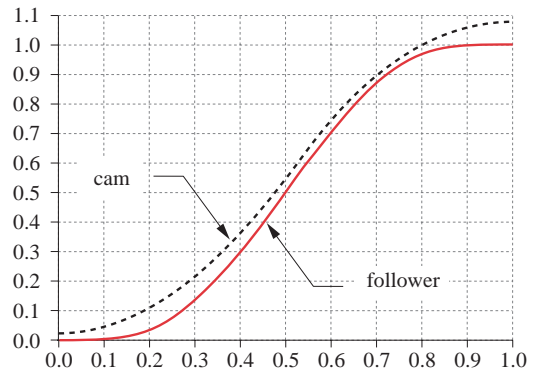
FIGURE 10-27

Dynamic response of double-dwell, 11th-degree polynomial functions, non-polydyne and polydyne cams

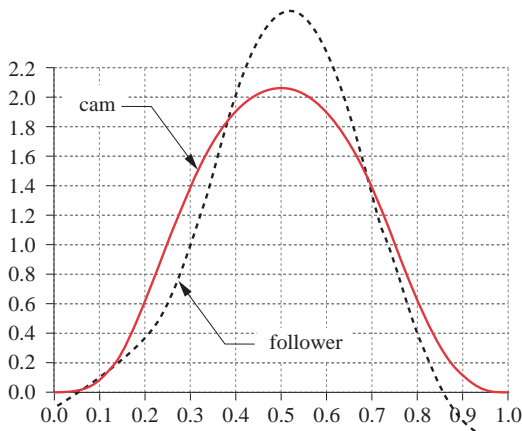
- 3 Apply the Runge-Kutta algorithm to solve this ODE for x and its derivatives, and solve for the dynamic force. The results are shown in Figure 10-27a. This non-polydyne cam undershoots its peak kinematic displacement by 0.020 in, overshoots its kinematic velocity and acceleration, and shows follower jump at 210° . The peak dynamic acceleration is 7138 in/sec^2 , 39% larger than the kinematic acceleration.
- 4 To determine the polydyne cam function needed to create the desired motion at the follower, substitute the kinematic displacement and its derivatives through ping (as defined by equations 10.28) into equations 10.20 for x and its derivatives, then solve for s and its first two derivatives. Figure 10-27b shows the dynamic displacement, velocity, acceleration, and force of this polydyne cam. This polydyne version of the same cam program shows well-controlled motion with a displacement error of only 0.003 in and only small errors in velocity and acceleration. These errors can be due to the lack of a damping term in equation 10.20. The peak follower acceleration is reduced to 5431 in/sec^2 , 6% larger than kinematic, and there is no follower jump.
- 5 Figure 10-28 shows the normalized kinematic displacement, velocity, and acceleration functions superposed on the corresponding dynamic responses of the follower rise for both the non-polydyne and polydyne cams. Figure 10-28a shows the dynamic displacement of the non-polydyne follower and the cam shoe kinematic displacement (labeled *cam*). The follower lags the cam shoe for the first half of the rise and falls short of the full kinematic displacement at the dwell. Figure 10-28b shows the difference in the polydyne cam shoe displacement and the follower displacement. Note that the polydyne cam shoe displacement is greater than the follower displacement over the entire rise to compensate for the dynamic deflection of the follower train.
- 6 Figure 10-28c shows the normalized kinematic velocity as imparted to the cam shoe and the resulting non-polydyne follower velocity that substantially overshoots the peak kinematic value. Figure 10-28d shows the polydyne cam shoe velocity, which initially leads the follower, and then lags it between about 25% and 75% of the rise period as the stored energy in the elastic follower train speeds up the follower mass. The follower velocity is nearly kinematic for the polydyne case.
- 7 Figure 10-28e shows the kinematic acceleration of the cam shoe and the resulting dynamic response of the follower for the non-polydyne cam. There is significant error coming off the previous dwell and a large overshoot in the follower acceleration response. In Figure 10-28f, the polydyne cam shoe acceleration function is distinctly different from that of the follower in order to compensate for system elasticity. The sudden drop in cam shoe acceleration during the start of the rise serves to slow the follower and control overshoot.
- 8 Note the "role reversal" of cam and follower between the polydyne and non-polydyne cam systems. The non-polydyne system has an "ideal" kinematic cam shoe motion but a distorted follower motion. The polydyne cam system deliberately distorts the cam shoe motion to compensate for system elasticity and mass, resulting in a follower motion that is closer to the kinematic ideal at the design speed. Vibration of the follower of a polydyne cam will be close to zero at the design speed as long as there is sufficient follower spring force to keep it in contact. The trade-off can be a cam contour with larger pressure angle, smaller radius of curvature, thus higher stresses, and even undercutting in severe cases.
- 9 It is reasonable to ask whether anything has been gained by using this polydyne approach over a more conventional one of, say, a modified trapezoidal (MT) acceleration motion program. After all, the MT will have a much lower theoretical kinematic acceleration



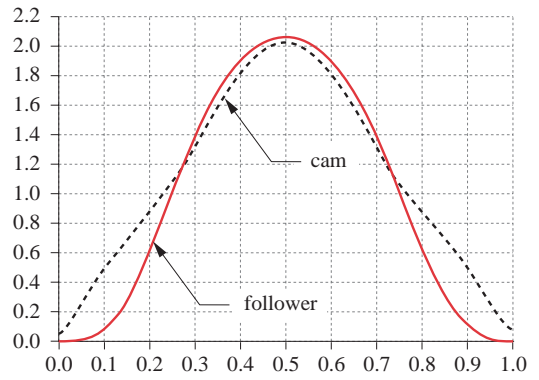
(a) Displacement of nonpolydyne cam and follower



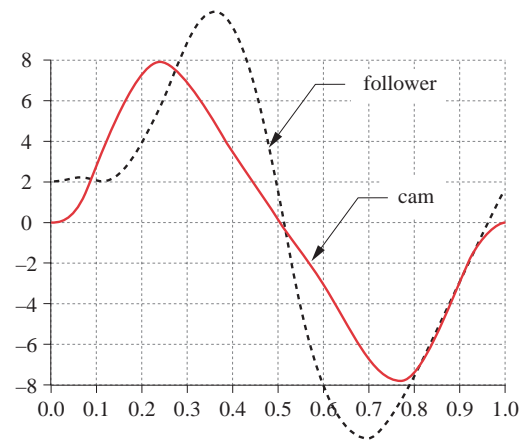
(b) Displacement of polydyne cam and follower



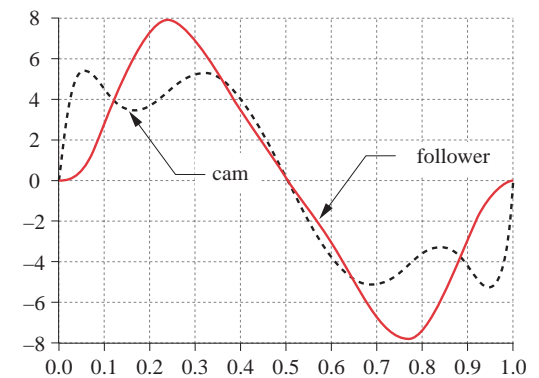
(c) Velocity factor for nonpolydyne cam and follower



(d) Velocity factor for polydyne cam and follower



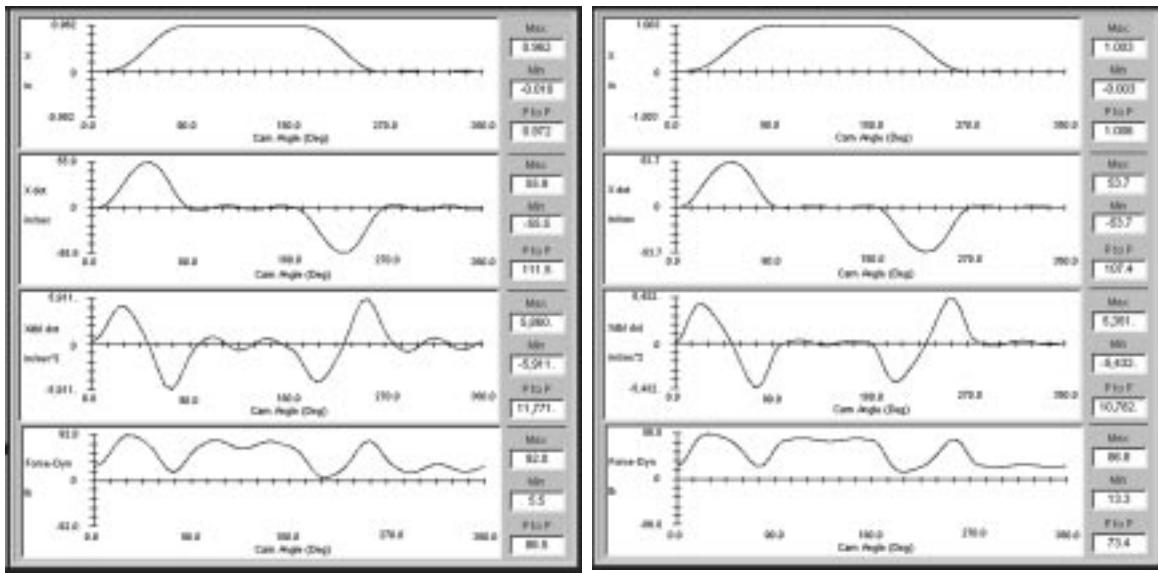
(e) Acceleration factor for nonpolydyne cam and follower



(f) Acceleration factor for polydyne cam and follower

FIGURE 10-28

Normalized double-dwell, 11th-degree polynomial functions, non-polydyne and polydyne cams



(a) Dynamic response of a modified trapezoid cam

(b) Dynamic response of a Peisekah polydyne cam

FIGURE 10-29

Dynamic response of double-dwell, non-polydyne modified trapezoid and 11th-degree polynomial polydyne cams

peak value ($3\,179\text{ in/sec}^2$) than the Peisekah polynomial used here (4.88 versus 7.91 acceleration factor). Figure 10-29 shows the dynamic displacement, velocity, acceleration, and force for an MT cam with the same lift and mass property specifications. It also shows the dynamic response of the polydyne cam from Figure 10-27b for comparison. Though the MT cam does not exhibit any follower jump (it comes close), it has a higher peak acceleration ($5\,955$ versus $5\,431\text{ in/sec}^2$) than the polydyne cam despite the lower theoretical acceleration of the MT. Thus, the real peak acceleration of the MT cam with this follower system is 87% higher than the MT kinematic acceleration and 10% higher than the polydyne cam. The peak dynamic force of the MT cam (92 lb) is also higher than the polydyne cam (87 lb) by 6%. Thus, the polydyne cam is a dynamically superior solution despite its 11th-degree polynomial function's theoretical disadvantages in terms of its higher kinematic peak values. Also note the lack of vibration of the polydyne cam during the dwells as compared to the MT. Overall, the polydyne cam is a better solution.

EXAMPLE 10-2

Designing a Polydyne Double-Dwell Cam With Closure Spring at Cam Follower.

Problem: Consider the following statement of a double-dwell motion problem:

| | |
|--------------|----------------------|
| Rise | 1 in over 90° |
| Dwell | for 90° |
| Fall | 1 in over 90° |

| | |
|--------------------|------------------------------|
| Dwell | for 90° |
| Speed | 180 rpm (3 Hz) |
| m_{eff} | 0.03 bl (11.6 lb) |
| k_1 | 1 000 lb/in for the linkage |
| k_2 | 50 lb/in at the end effector |
| Preload | 30 lb |
| ζ_1, ζ_2 | 0.05, 0.10, respectively |

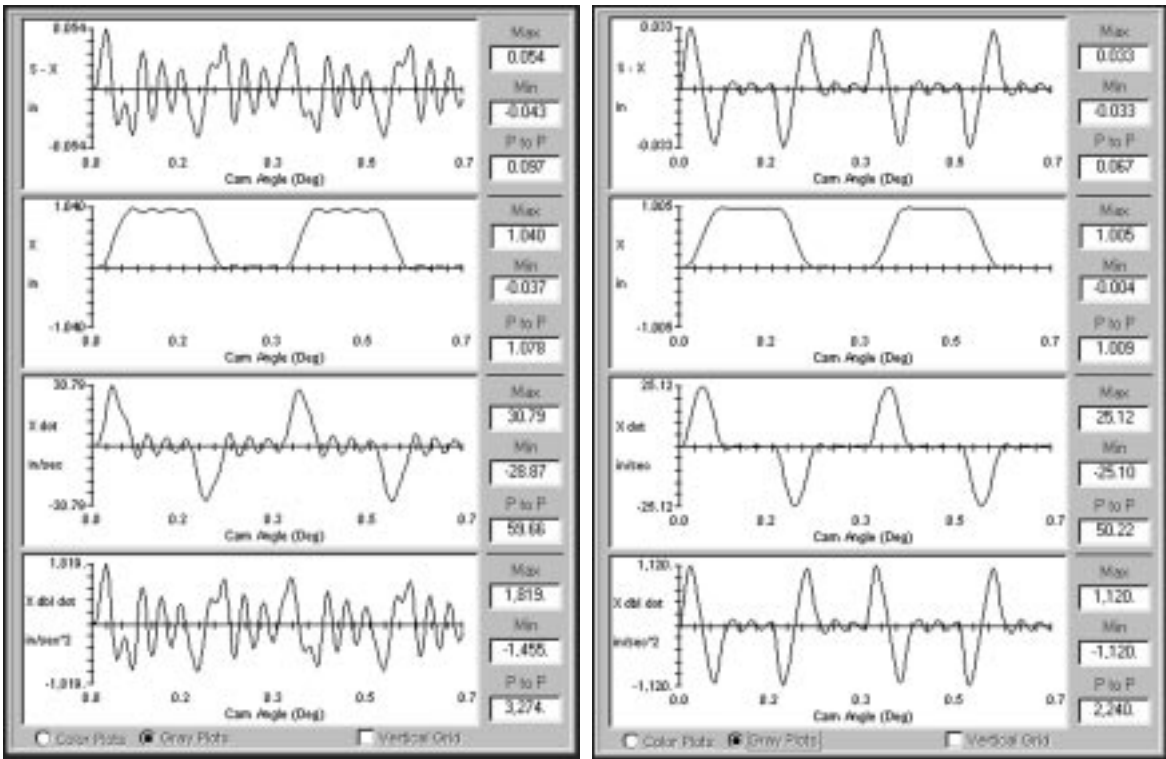
Assumptions: The joint closure spring is at the cam follower, so a SDOF, one-mass model as shown in Figure 10-8b (p. 276) will be used.

Solution:

- Figure 10-30 shows the difference between displacement, velocity, and acceleration of the follower for a non-polydyne and a polydyne cam with the same motion program, as calculated in program Dynacam. The motion is RDFD, 90-90-90-90 deg, with 1-in rise and fall at 180 rpm. A Peisekah 11th-degree polynomial is used on both rise and fall. The one-mass industrial cam dynamic model of Figure 10-8 is used with a return spring rate of 50 lb/in and a 30-lb preload. The stiffness of the follower train is 1 000 lb/in and the mass of the follower is 0.03 bl. Damping is between 0.05 and 0.1 of critical.
- Figure 10-30a shows the non-polydyne solution. Note the significant error in the follower's velocity and acceleration functions. The displacement overshoots by 0.034 in and undershoots by 0.036 in. The peak follower acceleration is 1 450 in/sec².
- Figure 10-30b shows the same data for a polydyne cam using the same Peisekah 11th-degree polynomial and equations 10.21. The velocity and acceleration functions now look like the theoretical functions, with the peak acceleration reduced to 1 121 in/sec². This is 1.5% lower than the designed kinematic acceleration of 1 138 in/sec², within the numerical error expected from the simulation. The displacement error is reduced to +0.005 / - 0.004 in. Some of this error is due to the absence of a damping term in equations 10.21.
- Figure 10-31 shows the kinetostatic and dynamic follower force functions superposed for each of the cases, non-polydyne and polydyne. In Figure 10-31a, the dynamic force is grossly different than the kinetostatic force and is close to zero at one point, indicating incipient jump. The polydyne cam contour has reduced the dynamic force significantly in Figure 10-31b. It is now close to the kinetostatic ideal and would be exactly equal if the damping were included in the polydyne equations and the dynamic model was exact.

10.9 SPLINEDYNE CAM FUNCTIONS

In Chapters 5 and 6 we showed how spline functions, particularly B-splines, can provide superior solutions to motion control problems than polynomials can in some cases. It would seem logical that splines then might offer some advantages to polydyne-type cam designs as well. The polydyne approach requires a function for the follower motion that has continuity through the 4th derivative of displacement, or ping. This is easy to accomplish with B-splines since they have the ability to control the unwanted excursions that are typical of high-order polynomials. Moreover, manipulation of knot locations can reduce peak velocity and acceleration. Thus, we introduce the concept of a splinedyne cam, a combination of spline functions for the motion and the dynamics of the follower train.



(a) Non-polydyne dynamic response

(b) Polydyne dynamic response

FIGURE 10-30

Non-polydyne and polydyne responses of a follower train to the same cam motion program

Figure 10-32 (p. 310) shows a 6th-order B-spline for a double-dwell rise motion with ten boundary conditions that make the displacement and its first four derivatives (through ping) zero at the beginning of the rise. At the end of the rise the displacement is equal to the total lift h , and its first four derivatives are zero. Choosing a 6th-order (5th-degree, quintic) spline for this motion leaves four internal knots available for manipulation and still provides continuity through ping. The functions in the figure were calculated with a camshaft speed of 1 rad/sec, a rise of 1 unit, and a period of 1 radian. This makes their peak values nondimensional, thus providing factors comparable to those of Table 3-2 (p. 50).

Pulling pairs of knots close to the beginning and end of the interval has the effect of forcing the displacement curve to rise (and fall) more rapidly at the extremes and so lowers the velocity and acceleration peaks (at the expense of peak jerk). The functions shown in Figure 10-32 have knots at points approximately 7% and 8% of the period in from each end, respectively. This gives a peak velocity factor of 2.1 and a peak acceleration factor of 7.1. These are better than the Peisekah polynomial of the previous sec-

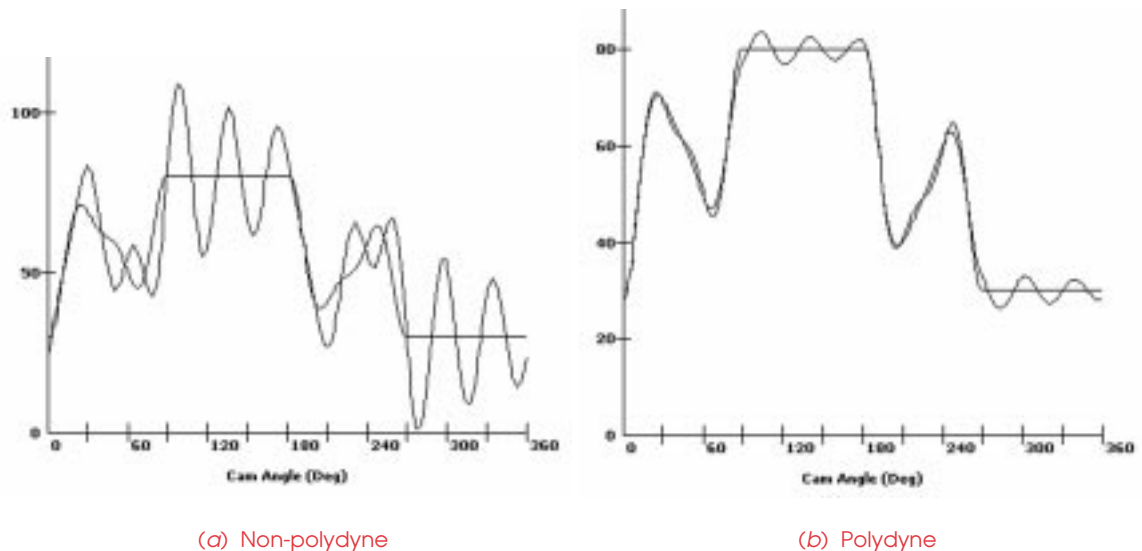


FIGURE 10-31

Kinetostatic and dynamic force for a polydyne and non-polydyne cam made to the same motion program

tion, and their peak values are not much higher than the classic cycloidal motion. But, because of their 4th-order continuity, these functions also have the ability to be modified according to the system's dynamics to provide a splinedyne, low-vibration motion at one design speed by using equations 10.20 or 10.22 (p. 292) to define the cam shape based on these follower motion functions.

Figure 10-33 (p. 311), shows an 8th-order B-spline for a double-dwell rise motion with the same ten boundary conditions as used in the functions of Figure 10-32. Now there are only two interior knots available for manipulation. These are placed 3.5% in from each end of the interval. Note that the functions through jerk and ping are much smoother than the 6th-order B-spline of Figure 10-32 due to the higher-order continuity of this spline. The penalty is higher peak factors, now 2.23 for velocity and 7.78 for acceleration, but comparable to the Peisekah 11th-degree polynomial.

EXAMPLE 10-3

Designing a Splinedyne Double-Dwell Cam With Spring at Cam Follower.

Problem: Consider the same double-dwell motion problem as in Example 10-2:

| | |
|--------------|-------------------|
| Rise | 1 in over 90° |
| Dwell | for 90° |
| Fall | 1 in over 90° |
| Dwell | for 90° |
| Speed | 180 rpm (3 Hz) |
| m_{eff} | 0.03 bl (11.6 lb) |

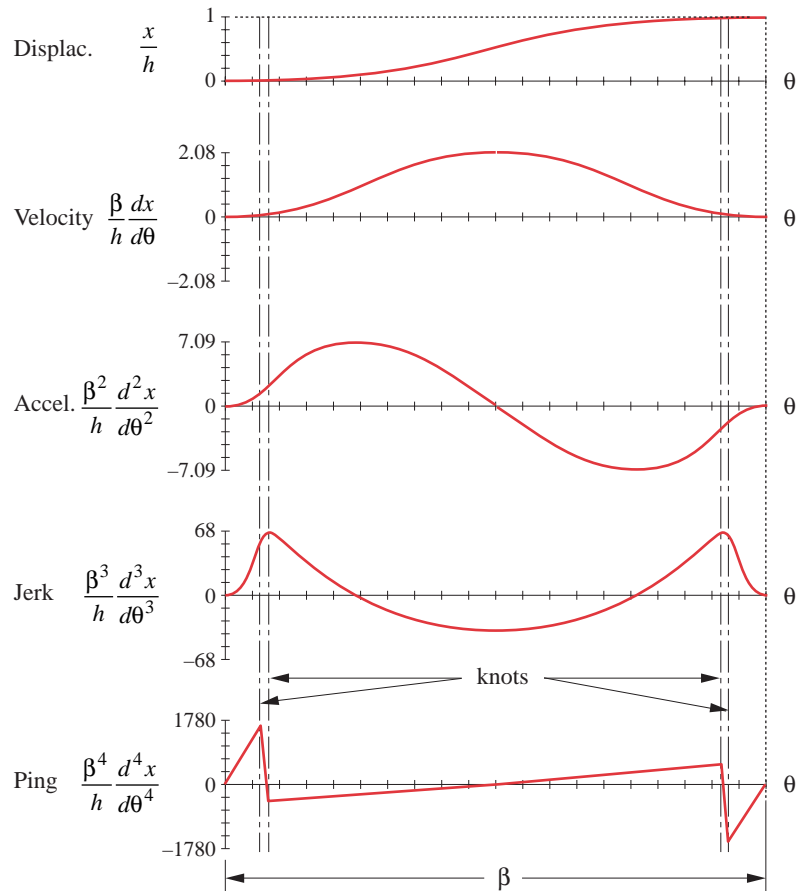


FIGURE 10-32

6th-order spline function for a splinedyne cam, knots at 7%, 8%, 92%, and 93% of period

| | |
|--------------------|------------------------------|
| k_1 | 1 000 lb/in for the linkage |
| k_2 | 50 lb/in at the end effector |
| Preload | 30 lb |
| ζ_1, ζ_2 | 0.05, 0.10, respectively |

Assumptions: The joint closure spring is at the cam follower, so a SDOF, one-mass model as shown in Figure 10-8b (p. 276) will be used.

Solution:

- Figure 10-34 (p. 312) shows the difference between displacement, velocity, and acceleration of the follower for a non-splinedyne and a splinedyne cam with the same motion program, as calculated in program DYNACAM. The motion is RDFD, 90-90-90-90 deg, with 1-in rise and fall at 180 rpm. The 8th order B-spline of Figure 10-33 is used on both rise and fall. The one-mass dynamic model of Figure 10-8 is used with a return spring rate

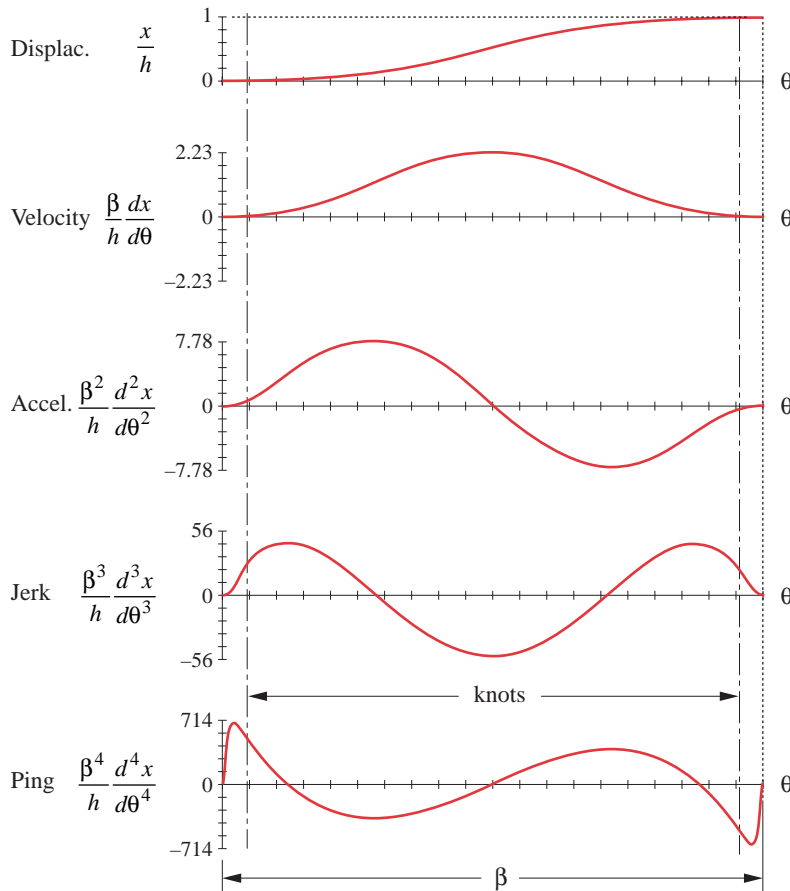
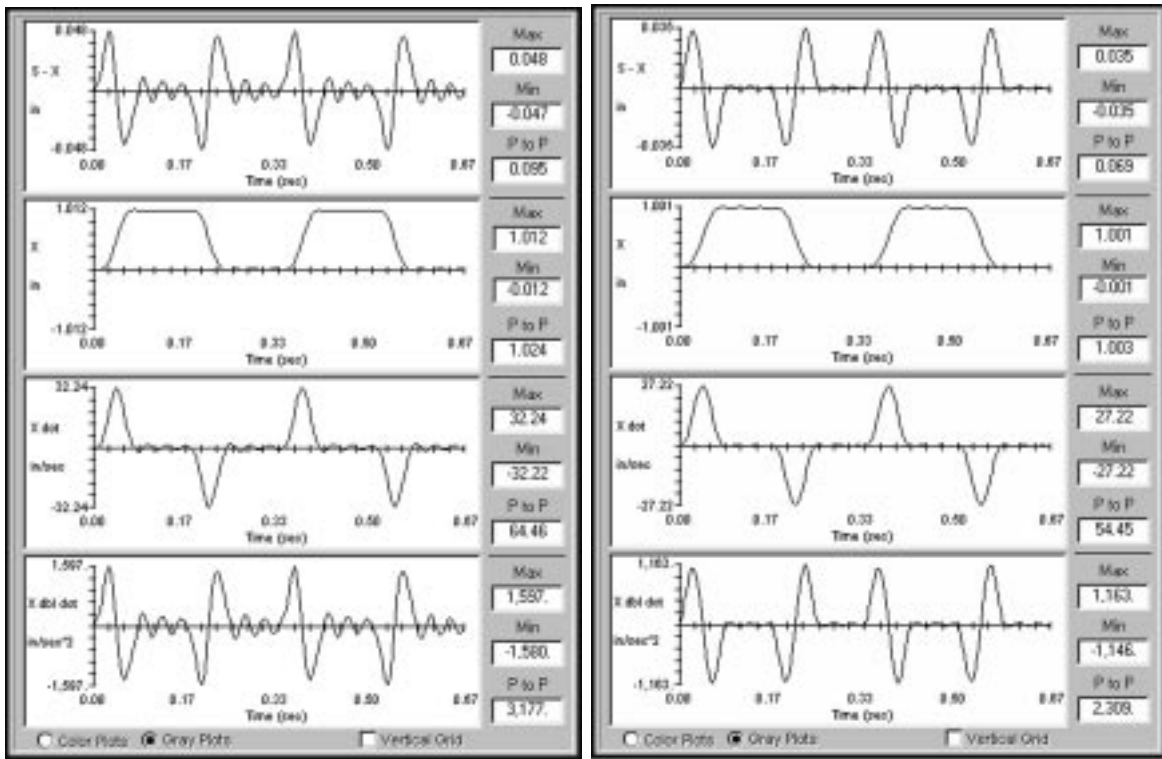


FIGURE 10-33

8th-order spline function for a splinedyne cam, knots at 3.5% and 96.5% of period

of 50 lb/in and a 30-lb preload. The stiffness of the follower train is 1 000 lb/in and the mass of the follower is 0.03 bl. Damping is between 0.05 and 0.1 of critical. All these data are identical to those used for the Peisekah polynomial of Example 10-2.

- 2 Figure 10-34a shows the non-splinedyne solution. There is less error in the follower's velocity and acceleration functions than for the polynomial solution, but they are nevertheless oscillatory. The displacement overshoots by 0.012 in and undershoots by 0.012 in. The peak follower acceleration is 1 600 in/sec².
- 3 Figure 10-34b shows the same data for the splinedyne cam. The velocity and acceleration functions now look very much like the theoretical functions, with the peak acceleration reduced to 1 166 in/sec². This is only 4% higher than the designed kinematic acceleration of 1 121 in/sec², within the numerical error expected from the simulation using equation



(a) Non-splinedyne dynamic response

(b) Splinedyne dynamic response

FIGURE 10-34

Non-splinedyne and splinedyne responses to the same cam motion program

10.21. The displacement error is reduced to ± 0.001 in, a better result than the polydyne cam.

- Figure 10-35 shows the kinetostatic and dynamic follower force functions superposed for each of the cases, non-splinedyne and splinedyne. In Figure 10-35a, the dynamic force is much different than the kinetostatic force, though not as bad as that of the Peisekah polynomial of Figure 10-31. The splinedyne cam contour in Figure 10-35b has reduced the dynamic force significantly. It is now very close to the kinetostatic ideal. These figures show the superiority of the splinedyne cam over the polydyne cam for reducing dynamic oscillations at any one design speed. Either is significantly better than a cam design that does not account for the dynamics of the follower system, however.

10.10 REFERENCES

- Barkan, P.** (1953). "Calculation of High Speed Valve Motion with a Flexible Overhead Linkage." SAE Transactions, 61, pp. 687-700.

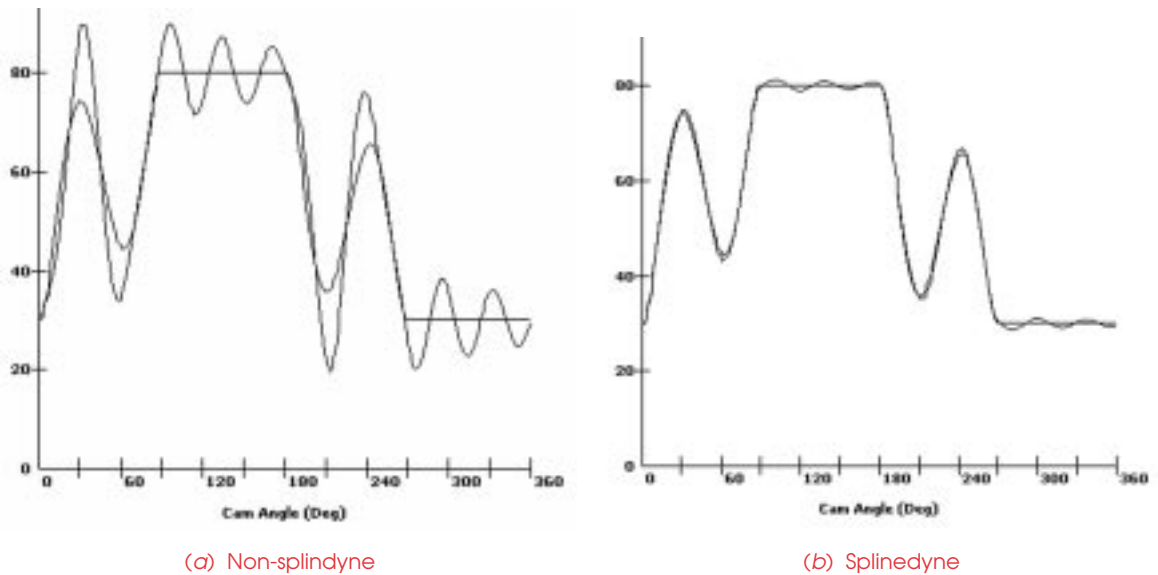


FIGURE 10-35

Kinestatic and dynamic force for a splinedyne and non-splinedyne cam made to the same motion program

- 2 **Koster, M. P.** (1974). *Vibrations of Cam Mechanisms*. Phillips Technical Library Series, Macmillan Press Ltd.: London.
- 3 **Akiba, K., and H. Sakai.** (1981). "A Comprehensive Simulation of High Speed Driven Valve Trains." 810865, SAE.
- 4 **Dresner, T. L., and P. Barkan.** (1995). "New Methods for the Dynamic Analysis of Flexible Single-Input and Multi-Input Cam-Follower Systems." *Journal of Mechanical Design*, 117(1), p. 151.
- 5 **Koster, M. P.** (1974). *Vibrations of Cam Mechanisms*. Phillips Technical Library Series, Macmillan Press Ltd.: London, p. 172.
- 6 **Seidlitz, S.** (1989). "Valve Train Dynamics - A Computer Study." 890620, SAE.
- 7 **Ibid.**, p. 11.
- 8 **Pisano, A. P.** (1981). "The Analytical Development and Experimental Verification of a Predictive Model of a High-Speed Cam-Follower System." Ph.D. Thesis, Columbia University.
- 9 **Ibid.**, p. 127.
- 10 **Wiederrich, J. L.** (1973). "Design of Cam Profiles for Systems with High Inertial Loading." Ph.D. Thesis, Stanford University.
- 11 **Norton, R. L.** (2000). *Machine Design: An Integrated Approach*. 2ed, Prentice-Hall: Upper Saddle River, NJ, pp. 111-116.

- 12 **Thoren, T. R., et al.** (1952). "Cam Design as Related to Valve Train Dynamics." SAE Quarterly Transactions, 6(1), pp. 1-14.
- 13 **Dudley, W. M.** (1948). "New Methods in Valve Cam Design." SAE Quarterly Transactions, 2(1), pp. 19-33.
- 14 **Stoddart, D. A.** (1953). "Polydyne Cam Design-I." Machine Design, January, 1953, pp. 121-135.
- 15 **Stoddart, D. A.** (1953). "Polydyne Cam Design-II." Machine Design, February, 1953, pp. 146-154.
- 16 **Stoddart, D. A.** (1953). "Polydyne Cam Design-III." Machine Design, March, 1953, pp. 149-164.
- 17 **Norton, R. L., et al.** (1999). "Effect of Valve-Cam Ramps on Valve Train Dynamics." SAE 1999-01-0801.
- 18 **Mosier, R. G.** (2000). "Modern Cam Design." Int. J. Vehicle Design, 23(1/2), pp. 38-55.
- 19 **Peisekah, E. E.** (1966). "Improving the Polydyne Cam Design Method." Russian Engineering Journal, XLVI(12), pp. 25-27.
- 20 **Fawcett, G. F., and J. N. Fawcett,** eds. (1978). "Comparison of Polydyne and Non-Polydyne Cams." Cams and Cam Mechanisms, Jones, J. R., ed., Institution of Mechanical Engineers: London.
- 21 **Press, W. H., et al.** (1986). *Numerical Recipes: The Art of Scientific Computing*. Cambridge University Press: Cambridge, pp. 547-577.